

# On the horseshoe drag of a low-mass planet. II Migration in adiabatic disks

F. S. Masset<sup>1,2</sup>

Laboratoire AIM, CEA/DSM - CNRS - Université Paris Diderot, Irfu/Service  
d'Astrophysique, Bât. 709, CEA/Saclay, 91191 Gif-sur-Yvette, France

`frederic.masset@cea.fr`

and

J. Casoli

Laboratoire AIM, CEA/DSM - CNRS - Université Paris Diderot, Irfu/Service  
d'Astrophysique, Bât. 709, CEA/Saclay, 91191 Gif-sur-Yvette, France

`jules.casoli@cea.fr`

Received \_\_\_\_\_; accepted \_\_\_\_\_

---

<sup>1</sup>Also at ICF-UNAM, Av. Universidad s/n, Cuernavaca, Morelos, C.P. 62210, México

<sup>2</sup>Send offprint requests to `frederic.masset@cea.fr`

## ABSTRACT

We evaluate the horseshoe drag exerted on a low-mass planet embedded in a gaseous disk, assuming the disk’s flow in the coorbital region to be adiabatic. We restrict this analysis to the case of a planet on a circular orbit, and we assume a steady flow in the corotating frame. We also assume that the corotational flow upstream of the U-turns is unperturbed, so that we discard saturation effects. In addition to the classical expression for the horseshoe drag in barotropic disks, which features the vortensity gradient across corotation, we find an additional term which scales with the entropy gradient, and whose amplitude depends on the perturbed pressure at the stagnation point of the horseshoe separatrices. This additional torque is exerted by evanescent waves launched at the horseshoe separatrices, as a consequence of an asymmetry of the horseshoe region. It has a steep dependence on the potential’s softening length, suggesting that the effect can be extremely strong in the three dimensional case. We describe the main properties of the coorbital region (the production of vortensity during the U-turns, the appearance of vorticity sheets at the downstream separatrices, and the pressure response), and we give torque expressions suitable to this regime of migration. Side results include a weak, negative feed back on migration, due to the dependence of the location of the stagnation point on the migration rate, and a mild enhancement of the vortensity related torque at large entropy gradient.

*Subject headings:* Planetary systems: formation — planetary systems: protoplanetary disks — Accretion, accretion disks — Methods: numerical — Hydrodynamics

## 1. Introduction

Planetary migration is the process by which forming planets undergo significant variations of their semi-major axis, as a result of the tidal interaction with the protoplanetary disk. The migration of low mass planets ( $M_p \lesssim 10 - 15 M_\oplus$ ), called type I migration, has long posed a problem for scenarios of planetary formation. Believed to be systematically inwards and fast (Ward 1986, 1997), the migration of these planets all the way to the central object should be much shorter than the disk’s lifetime. This raised the issue of why many planetary systems, including our own, harbor planets that are not very close to their star, and this triggered a lot of theoretical efforts, during the last decade, to exhibit mechanisms that would halt, or even reverse type I migration. Long thought to be isothermal (which noticeably simplified the analytical studies as well as numerical simulations), the tidal response of the disk was only recently considered in a more realistic manner, by including an energy equation. Morohoshi & Tanaka (2003) noticed that the disk’s response was significantly different in an optically thin disk (described in the approximation of the shearing sheet, in which there is no net torque between the planet and the disk), while Paardekooper & Mellema (2006) observed in high resolution, three dimensional calculations that increasing the opacity of the disk could halt or reverse the migration of low-mass planets. This result was subsequently interpreted, in the adiabatic limit, as a result of the advection of entropy within the horseshoe region (Baruteau & Masset 2008; Paardekooper & Papaloizou 2008), giving rise to a new term of the so-called horseshoe drag. This term is of crucial importance to theories of planetary migration since it may halt or revert migration (Baruteau & Masset 2008; Kley & Crida 2008; Paardekooper & Papaloizou 2008). While there is clearly a link between the advection of entropy and the existence of an additional term to the horseshoe drag, which undoubtedly scales with the radial gradient of entropy (Baruteau & Masset 2008), there is not yet a fully self-consistent treatment of the dynamics of the horseshoe region in an adiabatic disk. Even worse, it is

far from clear where the additional contribution originates. So far, it has been interpreted as due to overdense and underdense regions which appear at the horseshoe U-turns as the result of the advection of entropy in a disk that maintains a pressure balance. These regions are strikingly apparent in numerical simulations. They end abruptly, by a contact discontinuity, at the downstream separatrices (see e.g. Baruteau & Masset 2008). It is easy to realize that the contribution arising from the perturbed density in these regions scales with the entropy gradient, and has the correct sign (as inferred from numerical simulations). Nevertheless, a simple attempt to perform a full horseshoe drag calculation by integrating on the horseshoe streamlines reveals a paradox. The standard horseshoe drag calculation consists in integrating over the upstream flow, on each side of the planet, the mass flow rate inside of the stream tubes, multiplied by the jump of angular momentum experienced by the fluid particles that execute a horseshoe U-turn in these tubes (Ward 1991). The net result corresponds to the rate of exchange of angular momentum between the planet and the gas of the coorbital region. On the upstream side of the horseshoe U-turns, the mass flow rate is that of the unperturbed disk, and it cannot depend on the equation of state of the gas. Therefore, if the torque due to a given stream tube depends on the equation of state, this should be due to the fact that the jump of angular momentum during the horseshoe U-turn depends on the equation of state. For the sake of definiteness, consider the side of the horseshoe region where we expect the material to become underdense, and assume that the disk has a vanishing vortensity gradient. In order to decrease the density downstream of the horseshoe U-turns, the flow has essentially two possibilities: streamlines can move apart (hence horseshoe U-turns are not radially symmetric), or the velocity on the streamlines can differ from the Keplerian velocity, and in this case be larger than the Keplerian velocity in the corotating frame, so as to lead to an expansion of the material. In other words, a fluid particle originally on a streamline at  $-x = r - r_p$  ( $r$  being its orbital radius and  $r_p$  that of the planet) is not mapped to  $x$  but to  $x + \xi$ , and its velocity in the

corotating frame is not  $V = 2A(x + \xi)$  but  $V = 2A(x + \xi) + v$  (here  $A = (1/2)r\partial_r\Omega/\partial r$  is the first Oort’s constant, that quantifies the Keplerian shear at the planet’s orbit). The perturbed elongation  $\xi$  and perturbed velocity  $v$  adjust so as to create an underdense region downstream of the horseshoe U-turns. A simple relationship between  $\xi$  and  $v$  can be found using the conservation of the Bernoulli invariant in the corotating frame. For the sake of simplicity, we assume that here there is no pressure gradient, hence the variation of enthalpy during the horseshoe U-turn cancels out for an adiabatic flow. The conservation of the Bernoulli constant therefore reduces to the conservation of the Jacobi constant  $J$ , which reads  $J = V^2/2 + 2\Omega Ax^2$ . To lowest order in  $v$  and  $\xi$ , the conservation of the Jacobi constant yields  $2B\xi + v = 0$  (where  $B = \Omega + A$  is the second Oort’s constant). The jump of angular momentum of fluid elements is, to lowest order,  $\Delta j = 2r_p Bx + 2r_p B(x + \xi) + r_p v$ , hence it is  $\Delta j = 4r_p Bx$ , the very same value of the jump that is used in classical, barotropic estimates of the horseshoe drag. It seems therefore that there is no room, in a classical horseshoe drag formulation, for a dependence on the thermodynamics of the gas, whereas such dependence is evidenced by numerical simulations<sup>3</sup>. In this work we address this apparent contradiction. We lay out our assumptions, and define our notation and conventions in section 2. We introduce a formalism that leads to a rigorous horseshoe drag expression in section 3. This expression features a dependence on the entropy gradient, as expected. We call the corresponding term the adiabatic torque excess. We compare this adiabatic torque excess to results of numerical simulations in section 4. We present the features of the horseshoe region that most differ from the barotropic case in section 5. These are essentially the appearance of vorticity sheets at the downstream separatrices and a mild production of vortensity all over the downstream sides of the horseshoe region. We also

---

<sup>3</sup>Although our simple example is limited to a case with no pressure gradient and no vortensity gradient, we also expect an adiabatic torque excess in this case.

work out the pressure and density response over the coorbital region, and identify the term that is related to the adiabatic torque excess. In section 6, we give a simple interpretation of the origin of the adiabatic excess, and we provide suitable torque expressions in section 7. We then discuss additional issues in section 8, and draw our conclusions in section 9.

## 2. Prerequisite

### 2.1. Notation

We consider a planet of mass  $M_p$  orbiting a star of mass  $M_*$ , on a fixed circular orbit of radius  $a$  and of angular frequency  $\Omega_p$ . The planet is immersed in a gaseous protoplanetary disk, such that the planetary orbit is coplanar with the disk and prograde. We use  $\Sigma$  to denote the disk’s surface density,  $P$  to denote the vertically integrated pressure, and  $T$  to denote the vertically averaged temperature. We assume that the disk’s gas follows the ideal gas law, which reads:

$$P = \frac{\mathcal{R}\Sigma T}{\mu}, \quad (1)$$

in which  $\mathcal{R}$  is the ideal gas constant and  $\mu$  is the mean molecular weight. The disk isothermal sound speed is therefore:

$$c_s^{\text{iso}} = \sqrt{\frac{\mathcal{R}T}{\mu}}, \quad (2)$$

while adiabatic sound waves propagate at the speed:

$$c_s = \sqrt{\frac{\gamma\mathcal{R}T}{\mu}}, \quad (3)$$

where  $\gamma$  is the usual adiabatic index. We shall consider the gas entropy in two flavors.

The first of those, which we denote with a lower  $s$ , is oftentimes used in the astrophysical literature owing to its simplicity, as it reads:

$$s = \frac{P}{\Sigma\gamma}. \quad (4)$$

Nevertheless, we shall also need an expression for the entropy that is compliant with the original definition of entropy (the entropy exchanged is the heat exchanged divided by the temperature). We denote the latter with an upper  $S$ :

$$S = \frac{\mathcal{R}}{(\gamma - 1)\mu} \log \left( \frac{P}{\Sigma^\gamma} \right) = \frac{\mathcal{R}}{(\gamma - 1)\mu} \log s. \quad (5)$$

Another thermodynamics variable that we shall need is the enthalpy  $\eta$ , which reads for an ideal gas:

$$\eta = \frac{\mathcal{R}}{\mu} \cdot \frac{\gamma - 1}{\gamma} T. \quad (6)$$

In what follows we shall assume, for the sake of simplicity, that  $\mathcal{R}/\mu = 1$ , which amounts to changing the units of temperature, entropy and enthalpy, without loss of generality.

We note  $T_0$  the temperature of the unperturbed disk, which we assume to be uniform.

We identify a location in the disk by its distance  $r$  to the star and its azimuth  $\phi$  with respect to the planet. The gas has a radial velocity  $v_r$  and an azimuthal velocity  $v_\phi$  in the frame corotating with the planet (hence its angular frequency in an inertial frame is  $\Omega = v_\phi/r + \Omega_p$ ). The radius of corotation  $r_c$  is the location in the unperturbed disk where the material has same angular frequency as the planet:  $\Omega(r_c) = \Omega_p$ . We will make use of the distance  $x$  to corotation:  $x = r - r_c$ . We also consider the disk pressure scaleheight  $H = c_s/\Omega$ , and the aspect ratio  $h = H/r$ .

The gravitational potential exerted on the disk can be decomposed as the sum of the stellar potential  $\Phi_* = -GM_*/r$ , of the planetary potential  $\Phi_p$  and of the indirect potential  $\Phi_i$ . The expression of these last two terms are respectively:

$$\Phi_p = -\frac{GM_p}{(r^2 - 2ra \cos \phi + a^2 + \epsilon^2)^{1/2}}, \quad (7)$$

where  $\epsilon$  is the softening length of the planetary potential, and

$$\Phi_i = \frac{GM_p}{a^2} r \cos \phi = qa\Omega_p^2 r \cos \phi, \quad (8)$$

where  $q = M_p/M_*$ .

Using the notation of Baruteau & Masset (2008), we define the gradient of vortensity across corotation as:

$$\mathcal{V} = \frac{d \log(\Sigma/\omega)}{d \log r} = \frac{3}{2} + \frac{\Sigma_c}{r_c} \frac{d\Sigma}{dr} \Big|_{r_c}, \quad (9)$$

where  $\omega = (1/r)\partial_r(r^2\Omega)$  is the vertical component of the flow vorticity, and where  $\Sigma_c$  is the unperturbed surface density at the corotation radius. Note that instead of the vortensity properly speaking, which is  $\omega/\Sigma$ , we shall oftentimes consider its inverse,  $\Sigma/\omega$ . One reason for this choice is that, if we consider that the flow is that of the unperturbed disk, the perturbations of the inverse of the vortensity can directly be converted into perturbations of density, whose impact on the torque is straightforward. Finally, we define the gradient of entropy across corotation as:

$$\mathcal{S} = \frac{1}{\gamma} \frac{d \log s_0}{d \log r} = \frac{\gamma - 1}{\gamma} r \partial_r S_0. \quad (10)$$

## 2.2. Basic equations

The governing equations of the flow are the equation of continuity, the Euler equation and the energy equation, together with the closure relationship provided by the equation of state. The equation of continuity reads, in the frame corotating with the planet:

$$\partial_t \Sigma + \frac{1}{r} \partial_r(\Sigma r v_r) + \frac{1}{r} \partial_\phi(\Sigma v_\phi) = 0. \quad (11)$$

The Euler equations read, respectively in  $r$  and  $\phi$ :

$$\partial_t v_r + v_r \partial_r v_r + \frac{v_\phi}{r} \partial_\phi v_r - r \Omega_p^2 - 2\Omega_p v_\phi - \frac{v_\phi^2}{r} = -\frac{\partial_r P}{\Sigma} - \partial_r \Phi, \quad (12)$$

and

$$D_t j = -\frac{\partial_\phi p}{\Sigma} - \partial_\phi \Phi, \quad (13)$$

where  $D_t \equiv \partial_t + v_r \partial_r + \frac{v_\phi}{r} \partial_\phi$  and  $j = r^2 \Omega$  is the specific angular momentum. The equation of state that we adopt is that of ideal gases, which reads  $P = \Sigma T$ . In that case, the internal energy density is  $e = p/(\gamma - 1)$ , and the energy equation reads:

$$\Sigma D_t \left( \frac{e}{\Sigma} \right) = -p \vec{\nabla} \cdot \vec{v}. \quad (14)$$

This equation does not include source or sink terms of energy, as we assume the flow to be adiabatic.

### 2.3. Conventions

Since different authors represent the horseshoe region in different ways, we find it useful to refer to properties of this region in a manner independent of the representation. Orienting the azimuth rotation-wise, and assuming that, in the corotating frame, the planet is located at azimuth  $\phi = 0$ , we say that something occurs in front of the planet if it occurs at  $\phi > 0$ , and behind or on the rear side of the planet if it occurs at  $\phi < 0$ . Similarly, we refer to the upstream part of the horseshoe streamlines as the set of fluid elements that have not performed yet a horseshoe U-turn, whereas the downstream part correspond to the set of fluid elements that have already performed their U-turn.

### 2.4. Assumptions

Our main assumptions are as follows:

- We assume that there is only one stagnation point in the vicinity of the planet. This is usually not the case in barotropic situations, in which one has generally two X-stagnation points on the corotation, on each side of the planet (see e.g. Masset et al. 2006, or paper I). In the adiabatic case, nevertheless, we usually have only one

stagnation point, unless either the entropy gradient is very small, or the potential’s softening length is very small. We shall therefore assume in what follows that there is no ambiguity when we refer to the stagnation point. We will make some additional remarks on this assumption in section 8.1.

- We assume that the initial temperature field is uniform. This assumption is very similar to the assumption of global isothermality that is required in the isothermal case to carry out a rigorous horseshoe drag calculation (see paper I). This assumption is required in order for the quantity that we shall define in section 2.5 to be conserved along a fluid element’s path. We will mention in section 8.3 how our results can be generalized to the case of an arbitrary temperature profile.
- Finally, we assume that the flow is in steady state in the frame corotating with the planet, and that the flow upstream of the horseshoe U-turns is unperturbed. We note that these two assumptions are contradictory: reaching a steady state implies that the flow has executed many horseshoe librations, hence the upstream flow cannot be that of the unperturbed disk. Nevertheless, we restrict ourselves, in this analysis, to a study of the unsaturated torque value. This implies that we consider the flow on a time scale (i) longer than what it takes to execute a horseshoe U-turn, so that the flow has reached a steady state in some region of interest enclosing the planet, (ii) shorter than the horseshoe libration time, so that in the region of interest any fluid element has executed at most one horseshoe U-turn.

## 2.5. A useful invariant

We consider the Jacobi-like Bernoulli constant whose expression is, in steady state:

$$B_J = \frac{r^2(\Omega - \Omega_p)^2 + v_r^2}{2} + \Phi_* + \Phi_p + \Phi_i - \frac{1}{2}r^2\Omega_p^2 + \eta. \quad (15)$$

Since  $B_J$  is conserved along the path of a fluid element, the quantity defined as:

$$G = B_J - T_0 S \quad (16)$$

is also conserved in an isentropic flow. Far from the planet, assuming a purely azimuthal motion, we can write, from Eqs. (15) and (16):

$$\partial_r G = (\Omega - \Omega_p) r \omega + (T - T_0) \partial_r S, \quad (17)$$

where we have used the rotational equilibrium, which can be deduced from Eq. (12) by letting  $v_r \equiv 0$ , and which reads:

$$\partial_r \phi_* + \partial_r \eta = r \Omega^2 + T \partial_r S. \quad (18)$$

As a consequence, in the unperturbed flow ( $T \equiv T_0$ ),  $G$  is maximal at corotation, as is  $B_J$  in an isothermal disk, and it admits the following expansion to second order in  $x$ :

$$G = G_c + 2ABx^2, \quad (19)$$

where  $G_c$  is the value of  $G$  at corotation,  $A = (1/2)rd\Omega/dr$  is the first Oort's constant and  $B = (1/2r)d(r^2\Omega)/dr$  is the second Oort's constants, which are to be evaluated at corotation.

### 3. A horseshoe drag expression

#### 3.1. Initial formulation

We consider a domain  $D$  of the disk consisting of an angular sector centered on the star that encloses the planet, as depicted in Fig. 1. The azimuth of the boundaries (I) and (III) is chosen sufficiently large so that the material that crosses them can be considered to have a purely circular motion, while the boundaries (II) and (IV) enclose the horseshoe

region, and are chosen much further away from corotation than the horseshoe separatrices, so that they can be considered as circular. We note that in a real situation, this last requirement is hindered by the wake, which corresponds to epicyclic motion excited at Lindblad resonances. Nevertheless we discard this behavior in the present work, which amounts to considering an isolated corotation region. We want to avoid flux of material into the domain  $D$  through the boundaries (II) and (IV), so we adopt streamlines to define them. These two boundaries are therefore associated to some value of the  $G$  invariant. For convenience, we use the same value for  $G$  on both sides, and we note it  $G_\infty$ .

The torque exerted on the planet by the material included in the domain  $D$  reads:

$$\Gamma = \int \int_D \Sigma(\partial_\phi \Phi) d\phi r dr, \quad (20)$$

We can transform the integrand of Eq. (20) as follows:

$$\Sigma(\partial_\phi \Phi)r = -r\partial_\phi P - \partial_\phi(v_\phi \Sigma j) - \partial_r(r\Sigma v_r j), \quad (21)$$

where we have made use of the assumption of a steady state in the corotating frame, and where we have used Eqs. (11) and (13).

Since the boundaries of the domain  $D$  are sufficiently far from the planet that we can neglect radial motions, Eq. (20) can be recast as:

$$\Gamma = \left[ \int_{r_\infty^-}^{r_\infty^+} [rP + r(\Omega - \Omega_p)\Sigma j] dr \right]_F^R, \quad (22)$$

where  $r_\infty^+$  ( $r_\infty^-$ ) is the radius of the outer (inner) streamline that has  $G = G_\infty$ . The  $R$  and  $F$  notation at the right bracket of Eq. (22) means that the integration over  $r$  has to be performed respectively at the rear or front side of the domain  $D$  (boundaries III and I in Fig. 1). In Eq. (22), the first term of the integrand represents the pressure torque exerted on the material enclosed within the domain  $D$ , while the second term represents the budget

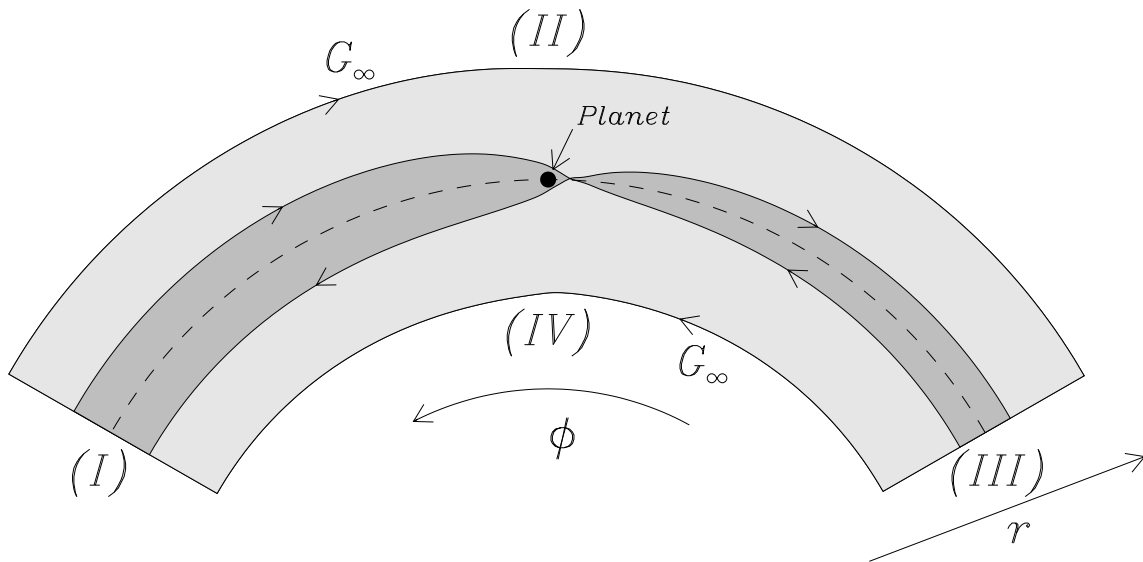


Fig. 1.— Sketch of the domain of integration (light grey) enclosing the horseshoe region (dark grey). The dashed line shows the corotation. As can be seen here, there is usually an offset between the planet, and the stagnation point of the horseshoe region (the point of intersection of the boundaries of the horseshoe region, i.e. the separatrices). There is also generally an offset between the corotation radius and the orbital radius of the planet, but it is much smaller.

of angular momentum brought to this region by advection. Since the flow is steady in the corotating frame, the angular momentum of this domain is constant in time and the torque is therefore integrally transmitted to the planet. We recognize in the second term of the integrand of Eq. (22) the classical horseshoe drag expression (Ward 1991, 1992; Masset 2001; Masset & Papaloizou 2003; Masset et al. 2006; Paardekooper & Papaloizou 2009a), but this equation also shows the pressure contribution, which has been overlooked in previous analysis.

### 3.2. A simplifying assumption

We assume that in the unperturbed flow, far from the planet, lines of constant entropy and of constant  $G$  coincide. This is not exactly true: in the unperturbed disk the lines of constant entropy are circles centered on the primary, while, owing to the presence of the potential’s indirect term given by Eq. (8), the iso- $G$  lines have a variable distance to corotation in the horseshoe region (an extreme example being provided by the tadpole separatrix). Our assumption is therefore more appropriate of a situation in which we discard the indirect term of the potential, or of a shearing sheet situation. Nevertheless, we shall make hereafter this assumption, anticipating that our torque expression does not depend sensitively on it.

This assumption allows to define unambiguously the derivative  $\partial_G S$ , which can be obtained from the measure of  $S$  and  $G$  on two neighboring streamlines, since these variables are intrinsic to the line. The quantity  $\partial_G S$  is therefore also intrinsic to the streamline, and hence conserved along it.

In the unperturbed disk, this derivative has the following expression:

$$\partial_G S = \frac{\partial_r S_0}{4ABx}. \quad (23)$$

It therefore diverges at corotation.

Mass conservation yields a relationship which will be useful to evaluate the production of vortensity during horseshoe U-turns. We consider a horseshoe stream tube, of width  $\delta G$ . The mass flux across the tube is:

$$\dot{M} = \frac{\delta G}{\partial_r G} r (\Omega - \Omega_p) \Sigma. \quad (24)$$

We can transform Eq. (17) to write:

$$(1 - \delta T \cdot \partial_G S) \partial_r G = (\Omega - \Omega_p) r \omega, \quad (25)$$

where  $\delta T = T - T_0$ . This eventually gives the mass flux:

$$\dot{M} = \delta G \frac{\Sigma}{\omega} (1 - \delta T \partial_G S). \quad (26)$$

We can therefore write the following relationship:

$$\frac{\Sigma}{\omega} (1 - \delta T \partial_G S) \Big|_d = \frac{\Sigma}{\omega} \Big|_u, \quad (27)$$

where the subscript  $d$  ( $u$ ) respectively denote the quantities downstream (upstream) of a horseshoe U-turn.

### 3.3. An alternate horseshoe expression

We now perform a change of variable in the integrals of Eq. (22). We choose as the new variable of integration the value of the  $G$  invariant. We have therefore to split the intervals of integration into intervals over which the dependency of  $G$  on  $r$  is continuous and monotonic. Anticipating on the results exposed in the following sections, we note that the value of the  $G$  invariant is not necessarily the same for the front and rear separatrices, as shown in Fig. 2. We denote their respective values with  $G_+$  and  $G_-$ .



Using Eq. (25), Eq. (22) is therefore recast as:

$$\begin{aligned}
 \Gamma = & \left[ \int_{r_{\infty}^{-}}^{r_{\infty}^{+}} r p dr + \int_{G_{\infty}}^{G_c} (1 - \delta T \partial_G S) \frac{\Sigma}{\omega} j dG \right. \\
 & + \left. \int_{G_c}^{G_-} (1 - \delta T \partial_G S) \frac{\Sigma}{\omega} j dG + \int_{G_+}^{G_{\infty}} (1 - \delta T \partial_G S) \frac{\Sigma}{\omega} j dG \right]_R \\
 & - \left[ \int_{G_{\infty}}^{G_-} (1 - \delta T \partial_G S) \frac{\Sigma}{\omega} j dG + \int_{G_+}^{G_c} (1 - \delta T \partial_G S) \frac{\Sigma}{\omega} j dG \right. \\
 & \left. + \int_{G_c}^{G_{\infty}} (1 - \delta T \partial_G S) \frac{\Sigma}{\omega} j dG + \int_{r_{\infty}^{-}}^{r_{\infty}^{+}} r p dr \right]_F
 \end{aligned} \tag{28}$$

We split the integration on the downstream side of the horseshoe U-turns in order to account for the possible discontinuity of  $G$  at the separatrices. More precisely, the first integral over  $G$  in Eq. (28) corresponds to an integral over intervals (1) and (2) (see Fig. 2), the two following integrals (from  $G_c$  to  $G_-$  and  $G_+$  to  $G_{\infty}$ ) correspond respectively to intervals (3) and (4). In a similar manner, on the front side, the intervals of integration over  $G$  are, in order of appearance, (5), (6) and eventually (7) and (8) together. We also note that in Eq. (28) we have substituted the total pressure  $P$  by the perturbed pressure  $p$ , since the unperturbed pressure field is axisymmetric and does not contribute to the pressure torque.

Other comments are in order regarding the transformation of Eq. (22) into Eq. (28). The integrand in Eq. (22) is regular, and although it may display discontinuities (we shall see that  $\Omega$  is discontinuous at the downstream separatrices, as well as  $\Sigma$ ) it does not contain any singularity. In contrast, the integrands of Eq. (28) feature the vorticity, which is singular wherever  $\Omega$  is discontinuous. Since the dependency of  $G$  upon  $r$  on the different intervals of integration is regular, the integrals on  $G$  must exclude any singularity (simply because the contribution of the integrand of Eq. (22) on any vanishingly small interval in  $r$  is vanishingly small, and the same must be true of the equivalent integral in  $G$ ). As a

consequence, any integral of Eq. (28) which has a boundary corresponding to a downstream separatrix must be understood as excluding the possible singularities at this boundary. For instance, the second integral over  $G$  in Eq. (28) must be understood as:

$$\int_{G_c}^{G_-} (1 - \delta T \partial_G S) \frac{\Sigma}{\omega} j dG \equiv \lim_{\delta G \rightarrow 0^+} \int_{G_c}^{G_- + \delta G} (1 - \delta T \partial_G S) \frac{\Sigma}{\omega} j dG. \quad (29)$$

We also note that including such singularities would be mathematically ill-defined anyway, because they lie on the edge of the integration domain.

Eq. (28) can be further simplified as explained below. The specific angular momentum  $j$  of a fluid element that has some value of the  $G$  invariant can be written as:

$$j = j_0 + \delta j, \quad (30)$$

where  $j_0$  is the specific angular momentum of fluid elements in the axisymmetric, unperturbed flow which have same value of  $G$ , and  $\delta j$  is the difference, that we wish to evaluate. Azimuthally far from the planet, Eq. (16) can be recast as:

$$G = \frac{r^2(\Omega - \Omega_p)^2}{2} + \Phi_* - \frac{1}{2}r^2\Omega_p^2 + \eta - T_0 S, \quad (31)$$

where we have neglected the indirect term (as discussed in section 3.2). Differentiating Eq. (31), we can write, to first order in the perturbation:

$$0 = r\delta r(\Omega^2 - 2\Omega\Omega_p) + r^2\delta\Omega(\Omega - \Omega_p) + \partial_r\Phi_*\delta r + \frac{p}{\Sigma_0}. \quad (32)$$

The left hand side of Eq. (32) cancels out because, as stated above, we consider a fluid element that has same value of  $G$  in the unperturbed flow and in the perturbed one. Using the rotational equilibrium of the unperturbed flow, and writing  $\delta P = \partial_r P_0 \delta r + p$ , we can recast Eq. (32) as:

$$0 = (\Omega - \Omega_p)\delta j + \frac{p}{\Sigma_0}. \quad (33)$$

We therefore have an expression for  $\delta j$  that involves the perturbation of pressure  $p$ . Since we consider the variation of angular momentum of a fluid element for a constant value

of  $G$ , it is natural to change to  $G$  the variable of the integrals of the pressure torque. The generic integrand of Eq. (28) therefore becomes:

$$\begin{aligned} \frac{\Sigma}{\omega}(1 - \delta T \partial_G S)j + \frac{rp}{\partial_r G} &= \frac{1}{\partial_r G}[\Sigma r(\Omega - \Omega_p)j_0(G) + \Sigma r(\Omega - \Omega_p)\delta j + rp] \\ &= \frac{\Sigma}{\omega}(1 - \delta T \partial_G S)j_0(G) + \frac{1}{\partial_r G} \frac{\Sigma_0 - \Sigma}{\Sigma_0} rp, \end{aligned} \quad (34)$$

where we have used Eqs. (25) and (33).

The last term of the right hand side of Eq. (34) cancels out to first order in the perturbation. Furthermore, the parity in  $\phi$  of the perturbed density and of the perturbed pressure (which will be studied in section 5.3) is such that the rear and front contributions of this term to Eq. (28) cancel out. Therefore we can discard the pressure torque in Eq. (28), provided we use the unperturbed value of the specific angular momentum  $j_0$ . Since  $G$  has a maximum at corotation, the notation  $j_0(G)$  contains an ambiguity, as one has to specify if  $j_0$  has to be evaluated inside or outside of corotation. In what follows we use the notation  $j_0^\pm$  to remove this ambiguity, and we drop the  $G$  dependency for the sake of brevity.

The fact that one can neglect the pressure torque and use the value of the unperturbed angular momentum has been demonstrated in paper I for isothermal disks. It is linked (i) to the fact that the evanescent pressure waves excited by the perturbation of the flow on the downstream side of the horseshoe U-turns do not alter the total horseshoe drag, even though they redistribute the perturbation of density and therefore change the local torque density, and (ii) to the fact that the impact on the torque of the rear-front asymmetry due to the feed back of the evanescent waves cancels out.

Using the simplification described above, we transform Eq. (28) as follows:

$$\Gamma = \left[ \int_{G_\infty}^{G_c} \frac{\Sigma}{\omega} \Big|_{0^-} j_0^- dG + \int_{G_c}^{G_-} \frac{\Sigma}{\omega} \Big|_{0^-} j_0^+ dG + \int_{G_+}^{G_\infty} \frac{\Sigma}{\omega} \Big|_{0^+} j_0^+ dG \right]_R \quad (35)$$

$$- \left[ \int_{G_\infty}^{G_-} \frac{\Sigma}{\omega} \Big|_{0^-} j_0^- dG + \int_{G_+}^{G_c} \frac{\Sigma}{\omega} \Big|_{0^+} j_0^- dG + \int_{G_c}^{G_\infty} \frac{\Sigma}{\omega} \Big|_{0^+} j_0^+ dG \right]_F .$$

Apart from discarding the pressure contribution and changing  $j$  into  $j_0$  in Eq. (35), we have introduced an additional simplification by making use of Eq. (27), and by referring to the unperturbed, upstream value of  $\Sigma/\omega(1 - \delta T \partial_G S)$ . We explicitly specify by the use of the index  $0^\pm$  whether the unperturbed vortensity must be considered outside or inside corotation.

We note (see Fig. 2) that the integrals over the intervals (1) and (5), on the one hand, and over the intervals (4) and (8) on the other hand, exactly cancel each other, hence the torque expression can further be reduced to:

$$\Gamma = - \int_{G_-}^{G_c} \frac{\Sigma}{\omega} \Big|_{0^-} \Delta j_0 dG + \int_{G_+}^{G_c} \frac{\Sigma}{\omega} \Big|_{0^+} \Delta j_0 dG, \quad (36)$$

where  $\Delta j_0 = j_0^+ - j_0^-$ . The corotation torque has therefore a very similar expression to the usual (barotropic) case, when integrated over a Bernoulli-like variable (Masset & Papaloizou 2003), except that the domain of integration does not have the same limits on the front side and on the rear side. Denoting by  $G_s$  the arithmetic mean of the neighboring values  $G_-$  and  $G_+$ , we can transform Eq. (36) into:

$$\Gamma \approx \int_{G_s}^{G_c} \left( \frac{\Sigma}{\omega} \Big|_{0^+} - \frac{\Sigma}{\omega} \Big|_{0^-} \right) \Delta j_0 dG - \frac{\Sigma_0}{2B} \Delta j_0^s \Delta G, \quad (37)$$

where  $\Delta j_0^s$  is the value of  $\Delta j_0$  for  $G = G_s$ , and where  $\Delta G = G_+ - G_-$ . The left term of the R.H.S. of Eq. (37) is the standard horseshoe drag, which scales with the vortensity gradient, and the right term, which we hereafter denote with  $\Gamma_1$ , is an additional contribution which arises from relaxing the barotropic hypothesis. Evaluating this contribution therefore amounts to evaluating  $\Delta G$ . This is the purpose of the following section.

### 3.4. Discontinuities at the stagnation point

The discontinuity in  $G$  that we wish to evaluate arises from the presence, at the downstream separatrices, of a contact discontinuity (see Fig. 2). Formally, an inspection of Eq. (15) and (16) reveals that this discontinuity can come, far from the planet, from a discontinuity in the enthalpy, in the entropy, and in the azimuthal velocity (the other terms being continuous across the separatrices). The situation becomes simpler at the stagnation point, where the velocity vanishes and where the discontinuity in  $G$  is entirely accounted for by a discontinuity of entropy and enthalpy. We have therefore:

$$\Delta G = \eta_+ - \eta_- - T_0(S_+ - S_-), \quad (38)$$

where the  $+$  ( $-$ ) sign refers to quantities outside, or in front of (inside, or behind) the stagnation point. Eq. (38) can be transformed into:

$$\Delta G = (s_+^{1/\gamma} - s_-^{1/\gamma}) \frac{\gamma}{\gamma - 1} P_s^{(\gamma-1)/\gamma} - \frac{T_0}{\gamma - 1} (\log s_+ - \log s_-), \quad (39)$$

where  $P_s$  is the value of the pressure at the stagnation point (this value is well-defined at this point, on the contrary to the other thermodynamics variables, since the pressure field is continuous). Using the first order expansions:  $s_+^{1/\gamma} - s_-^{1/\gamma} \approx (s_+ - s_-)s_0^{1/\gamma-1}/\gamma$  and  $\log s_+ - \log s_- \approx (s_+ - s_-)/s_0$ , we are led to:

$$\Delta G = \frac{1}{\gamma - 1} s_0^{1/\gamma-1} (P_s^{(\gamma-1)/\gamma} - P_0^{(\gamma-1)/\gamma}) (s_+ - s_-), \quad (40)$$

where  $P_0$  and  $s_0$  are the pressure and the entropy at the location of the stagnation point, in the unperturbed disk.

In the particular case of a small perturbation:  $|P_s - P_0| \ll P_0$ , the discontinuity in  $G$  takes the form:

$$\Delta G = \frac{1}{\gamma} \frac{p_s}{\Sigma_0} \frac{s_+ - s_-}{s_0}, \quad (41)$$

where  $p_s = P_s - P_0$  is the pressure perturbation at the stagnation point.

In order to proceed in the evaluation of  $\Delta G$ , we use the conservation of the  $G$  invariant along the upstream separatrices. At this stage of the derivation, we note that numerical simulations reveal that the horseshoe region in the adiabatic regime is rather asymmetric, so that the distance of the separatrices depend on the quadrant under consideration (rear vs. front, and upstream vs. downstream). Denoting with  $x_u^R$  the distance of the upstream separatrix from corotation on the rear side, we have, by evaluating  $G$  respectively on that separatrix far from the planet, by means of Eq. (19), and at the stagnation point:

$$G_- = G_c + 2AB(x_u^R)^2, \quad (42)$$

and

$$G_- = G_c - \eta_c + \eta_- + \Phi_p^s + T_0(S_c - S_-), \quad (43)$$

where  $\Phi_p^s$  is the planetary potential at the stagnation point,  $\eta_c$  and  $S_c$  are respectively the enthalpy and entropy at corotation in the unperturbed disk, and where we have used the relationship  $G_c = \Phi_*(r_c) - (1/2)r_c^2\Omega_p^2 + \eta_c - T_0S_c$  to derive Eq. (43). From Eqs. (42) and (43) we deduce:

$$2AB(x_u^R)^2 = \eta_- - \eta_c + \Phi_p^s + T_0(S_c - S_-). \quad (44)$$

In a similar manner, denoting with  $x_u^F$  the distance of the upstream separatrix from corotation on the front side, we have:

$$2AB(x_u^F)^2 = \eta_+ - \eta_c + \Phi_p^s + T_0(S_c - S_+). \quad (45)$$

From Eq. (40), we have:

$$\Delta G = \frac{1}{\gamma} \left[ \left( \frac{s_0}{s_{\pm}} \right)^{1/\gamma} \eta_{\pm} - \eta_c \right] \frac{s_+ - s_-}{s_0}, \quad (46)$$

hence we have:

$$2\Delta G = \frac{1}{\gamma} (\eta_+ + \eta_- - 2\eta_c) \frac{s_+ - s_-}{s_0}, \quad (47)$$

where we have discarded the additional term that scales with  $\mathcal{S}^2$ . Similarly, adding Eqs. (44) and (45) yields:

$$2AB[(x_u^R)^2 + (x_u^F)^2] = \eta_+ + \eta_- - 2\eta_c + 2\Phi_p, \quad (48)$$

where we have omitted the term  $T_0(2S_c - S_- - S_+)$ , which scales as  $h^2\Omega^2x^2$ , and is hence negligible compared to the left hand side. Using Eqs. (47) and (48), we obtain:

$$\Delta G = \frac{1}{\gamma} \left\{ AB[(x_u^R)^2 + (x_u^F)^2] - \Phi_p^s \right\} \frac{s_+ - s_-}{s_0} \quad (49)$$

Since the entropy is conserved during the advection along the upstream separatrices, we have:

$$\frac{s_+ - s_-}{s_0} = \gamma \mathcal{S} \frac{x_u^F + x_u^R}{a}. \quad (50)$$

The discontinuity of  $G$  reads finally:

$$\Delta G = \left\{ AB[(x_u^R)^2 + (x_u^F)^2] - \Phi_p^s \right\} \mathcal{S} \frac{x_u^F + x_u^R}{a} \quad (51)$$

and the associated torque excess is, using Eq. (37):

$$\Gamma_1 = -(x_u^F + x_u^R)^2 \Sigma_0 \mathcal{S} \left\{ AB[(x_u^R)^2 + (x_u^F)^2] - \Phi_p^s \right\}, \quad (52)$$

where we have used the equality  $\Delta j_0^s = 2Ba(x_u^R + x_u^F)$ . Since  $P_s > P_0$ ,  $\Delta G$  has same sign as  $\mathcal{S}$ , and the torque excess scales with the negative of the entropy gradient, as already observed in previous works (Baruteau & Masset 2008; Paardekooper & Papaloizou 2008).

We can render Eq. (52) a bit more compact by defining the averaged upstream half-width:

$$x_s = \sqrt{\frac{(x_u^R)^2 + (x_u^F)^2}{2}} \quad (53)$$

Considering that the relative asymmetry between the rear and front part of the horseshoe, albeit larger than typically observed in barotropic situations (see paper I), remains moderate, we have:

$$x_s \approx \frac{1}{2}(x_u^R + x_u^F), \quad (54)$$

and therefore:

$$\Gamma_1 \approx -4x_s^2 \Sigma_0 \mathcal{S} (2ABx_s^2 - \Phi_p^s), \quad (55)$$

This expression displays explicitly the dependency of the torque excess on the entropy gradient. As we shall see hereafter, it also brings in a dependency on the potential’s softening length, as both  $x_s$  and  $\Phi_p^s$  depend on this quantity.

#### 4. Comparison to numerical simulations

We have undertaken a number of numerical simulations in order to test the validity of Eq. (55), which quantifies the adiabatic torque excess. We briefly describe the code used and the parameters adopted, then we assess the correctness of Eq. (55) from series of calculations in which we vary the entropy gradient or the softening length.

##### 4.1. Numerical set up

We used the code FARGO<sup>4</sup> (Masset 2000a,b; Baruteau & Masset 2008) in its adiabatic and isothermal versions. Unless otherwise stated, the polar mesh extends from  $r_{\min} = 0.4$  to  $r_{\max} = 1.8$ , and has a resolution of  $1200 \times 1200$ , the zone boundaries being evenly spaced. The planet is located at  $r = 1$ , and it is held on a fixed circular orbit. Its mass ratio to the primary is  $q = 3 \cdot 10^{-6}$  (*i.e.* the planet has one Earth-mass, if the central object has a solar mass). The disk aspect ratio at  $r = 1$  is  $h = 0.05$ . The adiabatic index of the gas is  $\gamma = 1.4$ . Damping boundary conditions (as described in de Val-Borro et al. 2006) are used at the

---

<sup>4</sup>See: <http://fargo.in2p3.fr>

inner and outer edges of the mesh. The frame corotates with the planet, and the Coriolis force is conservatively implemented (Kley 1998). The surface density is a power law of the radius:  $\Sigma(r) \propto r^{-\sigma}$ .

In our first set of calculations, the slope of the surface density is set to  $\sigma = +3/2$  (hence the vortensity related part of the corotation torque cancels out), and the potential softening length ranges from  $\hat{\epsilon} = 0.1$  to 10. The logarithm of  $\hat{\epsilon}$  is evenly spaced, and 21 calculations are performed, so that  $\hat{\epsilon} = 10^{i/10-1}$ , with  $0 \leq i \leq 20$ . These calculations were performed both for an adiabatic flow (for brevity we denote them with EA $_{i,0 \leq i \leq 20}$ ) and for an isothermal flow (we denote them with EI $_{i,0 \leq i \leq 20}$ ). Since the initial temperature field is flat, the index of the entropy gradient is  $\mathcal{S} = \sigma(\gamma - 1)/\gamma = +3/7$ . We therefore expect a negative torque excess in the adiabatic case.

In our second set of calculations, the slope of the surface density ranges from  $\sigma = -4$  to  $\sigma = 4$ , the softening length being kept fixed at  $\hat{\epsilon} = 0.3$ . We have divided the slope interval into 41 calculations such that  $\sigma_i = -4 + 0.2 \times i$  ( $0 \leq i \leq 40$ ). These calculations were performed both for an adiabatic flow (we denote them with SA $_{i,0 \leq i \leq 40}$ ) and for an isothermal flow (we denote them with SI $_{i,0 \leq i \leq 40}$ ). Since the initial temperature field is flat, the index of the entropy gradient is

$$\mathcal{S} = \frac{\gamma - 1}{\gamma} \sigma. \tag{56}$$

It therefore ranges from  $-8/7$  to  $+8/7$ .

## 4.2. A note on the half width of the horseshoe region

As underlined in section 3.4, the horseshoe region in adiabatic calculations is more asymmetric than in the isothermal case. It also has a different dependence, more complex, on the disk parameters. This can be seen in Fig. 3, in which we plot the different values of

$x_s$  inferred from a streamline analysis on the runs of the series  $SA_i$ . In particular, the naive expectation that

$$x_s^{\text{adi}} = x_s^{\text{iso}}/\gamma^{1/4} \quad (57)$$

is true only in the barotropic case ( $\mathcal{S} = 0$ ). For non-vanishing entropy gradients, the averaged upstream half width exhibits a V-shaped dependence on  $\mathcal{S}$ , whereas the isothermal case is insensitive to this parameter. This more complex dependence of the width of the horseshoe region has a consequence on the evaluation of the torque excess. A simple estimate of the latter is:

$$\Gamma_1^r = \Gamma^A - \frac{\Gamma^I}{\gamma}, \quad (58)$$

but this estimate assumes  $x_{s,\text{adi}} = x_{s,\text{iso}}/\gamma^{1/4}$ , so that one gets rid of the vortensity related part of the horseshoe drag, retaining only the excess. This is not exactly true, since the adiabatic case has a horseshoe region in general larger than expected. In order to fully eliminate the vortensity part of the estimate, one should therefore use the expression:

$$\Gamma_1^c = \Gamma^A - \frac{\Gamma^I}{\gamma} - \frac{3}{4} \mathcal{V} \Omega_p^2 \Sigma_0 \left( x_{s,\text{adi}}^4 - \frac{x_{s,\text{iso}}^4}{\gamma} \right) \quad (59)$$

We shall hereafter refer to the estimate given by Eq. (58) as the rough or global estimate (hence the  $r$  superscript), and to the estimate of Eq. (59) as the corrected estimate (hence the  $c$  superscript).

### 4.3. Dependence on the softening length

We compare the torque excess, when  $\hat{\epsilon}$  varies, as provided by Eq. (55) and as provided by a direct comparison of the torque value in adiabatic and isothermal calculations. The results are presented in Fig. 4. We see that there is a good overall agreement between the direct measure of  $\Gamma_1^c$  and the result of Eq. (55), as the relative difference is at most  $\sim 10\%$  over the range  $0.1 \leq \hat{\epsilon} \leq 1$ . The value of  $x_s$ , as measured on the output at  $t = 40$  orbits and

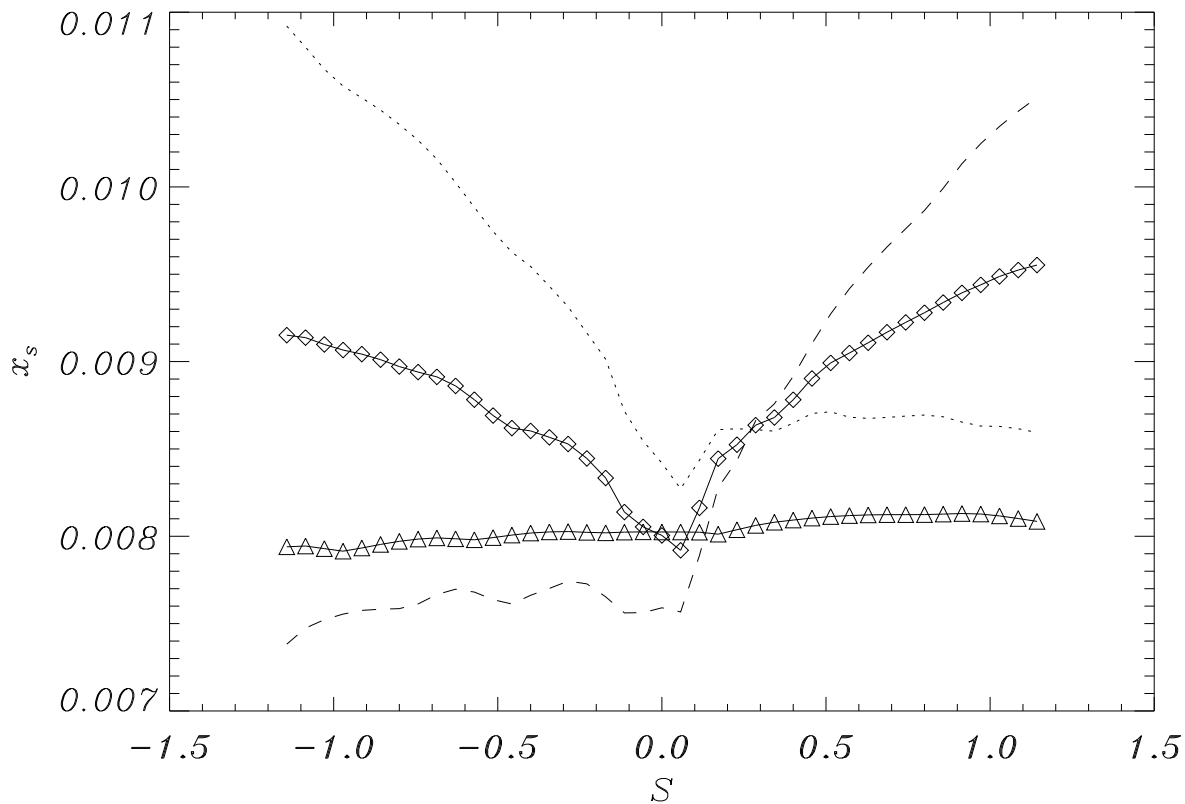


Fig. 3.— Half width  $x_s$  of the horseshoe region in the adiabatic case (diamonds), as a function of the entropy gradient  $\mathcal{S}$ . We use the arithmetic mean of  $x_u^R$  and  $x_u^F$  as an estimate of  $x_s$ . The dotted line shows  $x_u^F$ , and the dashed line shows  $x_u^R$ . The triangles show the half width of the horseshoe region (divided by  $\gamma^{1/4}$ ) obtained from runs with same parameters, but with an isothermal equation of state. The rear/front averaged upstream half width has a characteristic V-shape. The data presented here are obtained from the series of runs SA and SI.

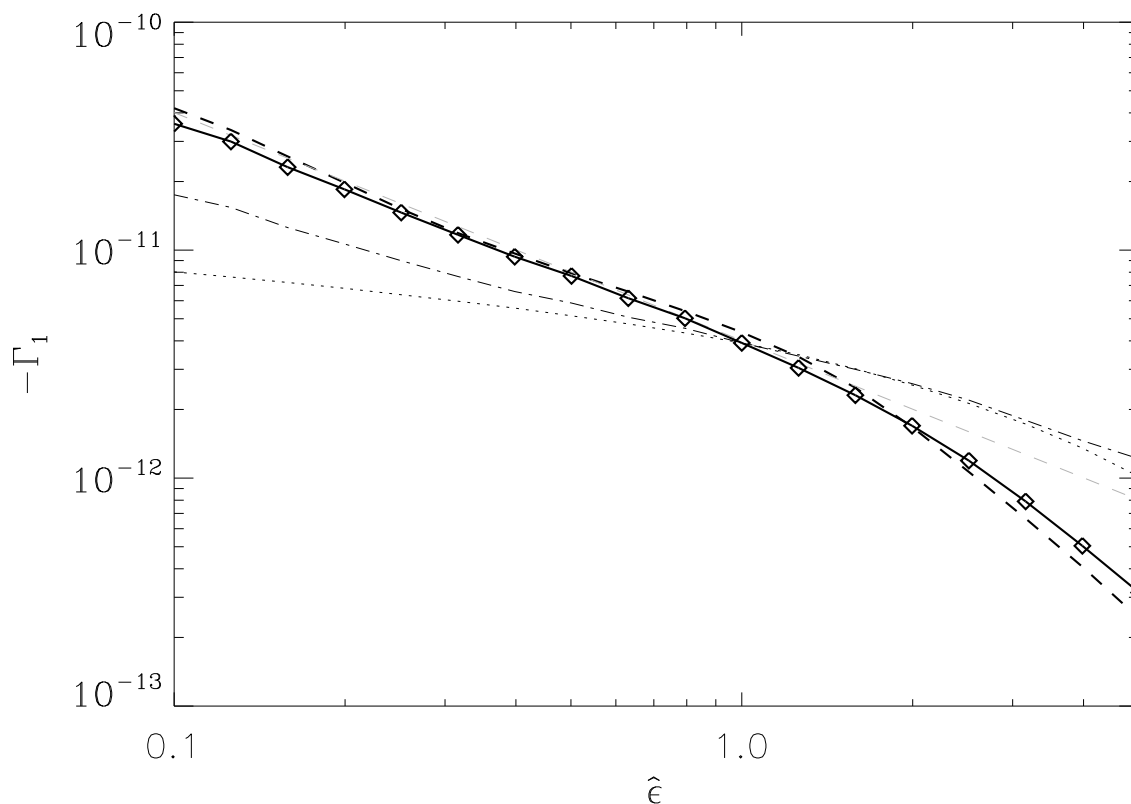


Fig. 4.— Torque excess as a function of the softening length. The thick dashed line shows the excess  $\Gamma_1^c$  directly measured by comparing the runs  $EA_i$  and  $EI_i$ , by means of the Eq. (59) – or (58), since the vortensity gradient is zero in this series of runs –, while the thick curve with diamonds shows the prediction of Eq. (55). The dash-dotted and dotted curves show the result of Eq. (55) in which one respectively adopts a constant value for  $x_s$  or for  $\Phi_p^s$  (namely the value measured for  $\hat{\epsilon} = 1$ ). The grey dashed line shows the prediction of Eq. (96), which will be derived in section 7.

$\phi = \pm 1$  rad, is used in the evaluation of Eq. (55). Similarly, the location of the stagnation point is determined, and used to evaluate the planetary potential that features in the bracket of Eq. (55). We note that in all the runs of this series, there is a unique stagnation point in the planet’s vicinity, hence there is no ambiguity in its determination.

There is an approximate  $\hat{\epsilon}^{-1}$  scaling of the torque excess in the range  $0.1 \leq \hat{\epsilon} \leq 1$  (Baruteau 2008). Fig. 4 shows that this trend results partly from the increase of  $x_s$  as  $\hat{\epsilon}$  decreases (dotted curve), and partly from the increase (in absolute value) of the planetary potential as the softening length decreases (dot-dashed line).

#### 4.4. Dependence on the entropy gradient

We now evaluate how well Eq. (55) accounts for the torque excess in the second series of runs (SA and SI, see section 4.1), in which we vary the entropy gradient.

The results are presented in Fig. 5. They show a satisfactory agreement between the corrected estimate of the torque excess (given by Eq. [59], and represented by the thick dashed line), and the theoretical prediction of Eq. (55), represented by the thick solid line. This figure also shows that the azimuth of the stagnation point oscillates as the entropy gradient varies. The oscillations are significantly large, and can be unambiguously identified as a finite resolution issue, for the following reasons:

- when the entropy gradient varies, the corotation radius is slightly shifted. If one displays the azimuth of the stagnation point as a function of the corotation radius, the period of the oscillations is equal to the radial resolution.
- We have carried out higher resolution calculations ( $2000 \times 2000$ , not shown here, as they were performed over a small number of orbits and a steady state was not reached in the vicinity of the planet), which were ran for 10 orbits only (the location of the

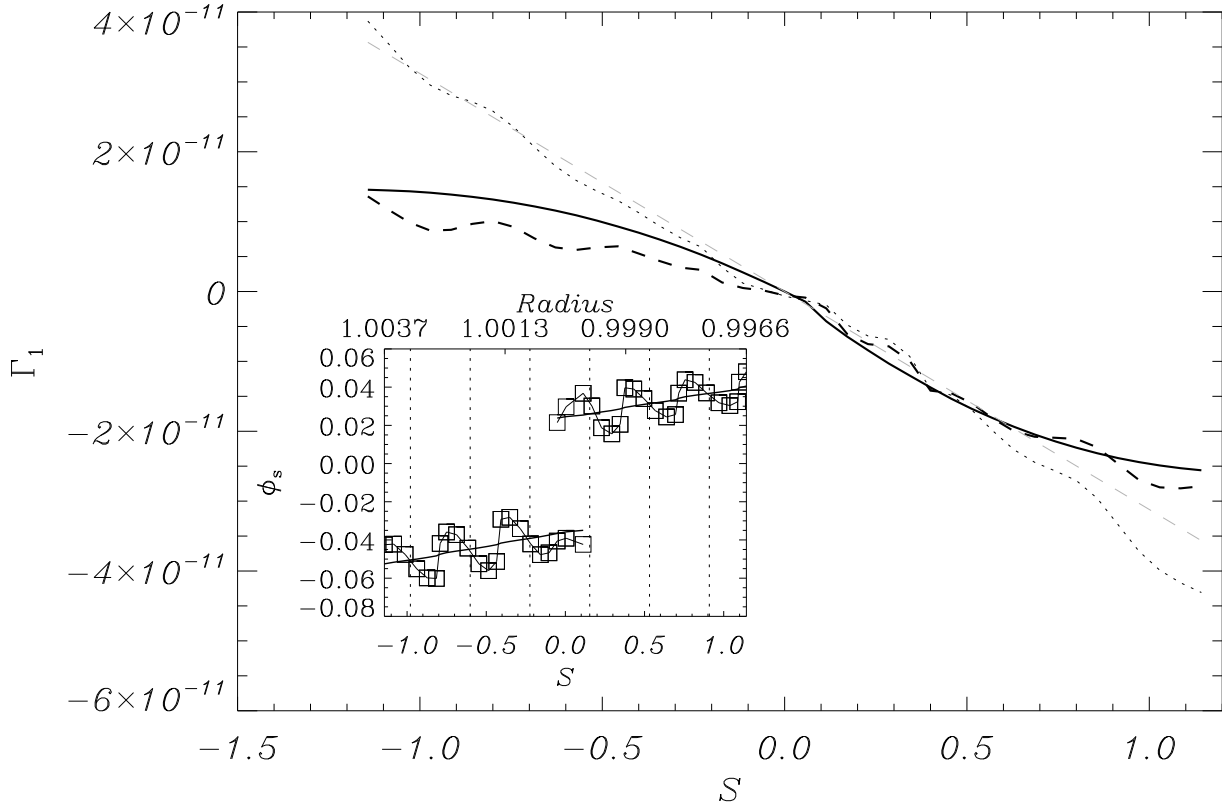


Fig. 5.— Torque excess as a function of the entropy gradient. The thick dashed line shows the corrected direct estimate  $\Gamma_1^c$  given by Eq. (59), while the thin dotted line shows the rough estimate  $\Gamma_1^r$  of Eq. (58). The thick solid line shows the result of Eq. (55), in which we use the planetary potential at the stagnation point and the horseshoe width, given by a prior streamline analysis performed at  $t = 40$  orbits for each calculation (and corrected as explained in the text). The inset plot shows the azimuth of the stagnation point, as a function of the entropy gradient (lower axis) and as a function of the corotation radius (upper axis). The vertical dotted lines show the zone boundaries. The thick solid lines of the inset plot shows linear regression fits of the stagnation point location, aimed at getting rid of the spurious oscillations. These fits were used in Eq. (55) and gave the thick solid curve of the main plot. The grey dashed line shows the prediction of Eq. (96), which will be derived in section 7.

stagnation point hardly varies afterwards). They also yield oscillations of the azimuth of the stagnation point with a shorter period and smaller amplitude.

Given the large amplitude of the oscillations of the stagnation point for the resolution that we were able to use for this series of runs, we need to smooth the  $\phi_s(\mathcal{S})$  function. This is done simply by performing a linear regression fit, independently for the rear and front stagnation points, as shown in the inset plot of Fig. 5. The fitted values are then used in Eq. (55), which yields the solid thick curve.

The value of  $\mathcal{S} = +3/7$  used in the series of runs EA and EI corresponds to a location where the error due to the oscillations of the azimuth of the stagnation point is small. We therefore understand from this plot why there is a good agreement between the measured and predicted adiabatic excess in Fig. 4. The fact that there is a good agreement for all values of  $\hat{\epsilon}$  in Fig. 4 suggests that the error on the location of the stagnation point is essentially due to the location of the corotation with respect to the mesh (which does not depend on the softening length). We recover the fact that, for  $\hat{\epsilon} = 0.3$ ,  $|\Gamma_1| \sim 1.5 \cdot 10^{-11}$ .

It is noteworthy that, on the left part of the plot of Fig. 5, there is a sizable difference between the rough and corrected estimates of the excess (thick dashed curve and dotted curve). The reason for this is straightforward, since for these values of the entropy gradient, the surface density increases steeply outwards, hence the vortensity related corotation torque is large and positive. For large values of  $|\mathcal{S}|$ , the adiabatic horseshoe half width is significantly larger than  $x_s^{\text{iso}}/\gamma^{1/4}$  (see section 4.2), therefore a fair fraction of the adiabatic excess is actually due to the boost of the vortensity related torque.

## 5. Properties of the coorbital region

We describe in this section the properties of the coorbital region that differ from the barotropic case. The most salient feature is the appearance of vorticity sheets along the downstream separatrices. We also derive the production of vortensity within the horseshoe region. The latter is weak, however, and does not have any impact on the horseshoe drag. We finally discuss the properties of the pressure disturbances arising from the horseshoe dynamics, and identify which component of these is responsible for the adiabatic torque excess.

### 5.1. Vorticity sheets

The discontinuity of the  $G$ -invariant that we evaluated in section 3.4 at the stagnation point also exists along the downstream separatrices, as can be seen in Fig. 2. Far from the planet, one can write the expression of the  $G$  discontinuity across a downstream separatrix as:

$$\Delta G = \frac{1}{\gamma \Sigma_0} \frac{p'_s}{s_0} \frac{s_+ - s_-}{s_0} + \frac{r^2}{2} [(\Omega_+ - \Omega_p)^2 - (\Omega_- - \Omega_p)^2], \quad (60)$$

where we have performed the same series of transformations as in Eqs. (38) to (41), where  $p'_s$  is the perturbed pressure at the separatrix, and where  $\Omega_+$  ( $\Omega_-$ ) is the angular velocity on the outside (inside) of the separatrix. If we assume in a first approximation that the perturbation of pressure at the separatrix, far from the planet, is much smaller than at the stagnation point, most of the  $G$ -discontinuity is ensured by the jump of azimuthal velocity, i.e. by a vorticity sheet. Denoting with  $\Delta v = r(\Omega_+ - \Omega_-)$  the magnitude of the vorticity sheet (i.e. the singular part of the flow's vorticity reads:  $\omega = \Delta v \delta(x - x_s)$ , where  $\delta$  is Dirac's delta function), and assuming that the jump is sufficiently small so that we can write:

$$\Omega_+ + \Omega_- - 2\Omega_p = \frac{4Ax}{a}, \quad (61)$$

we are led to:

$$\Delta v = \frac{\Delta G}{2Ax} = \begin{cases} \frac{\Gamma_1}{4a|A|x_s^2\Sigma_0} & \text{at the rear separatrix} \\ -\frac{\Gamma_1}{4a|A|x_s^2\Sigma_0} & \text{at the front separatrix} \end{cases} \quad (62)$$

Therefore, if there is a positive torque excess (hence  $\mathcal{S} < 0$ ), then there is a negative (positive) vorticity sheet in front of the planet (at the rear of the planet), and vice-versa. In order to illustrate this, we show in Fig. 6 the vorticity field in a run with  $\mathcal{S} = 1/3$  and similar characteristics as those of section 4.1, except that the resolution was set to a 2000 zones in azimuth and 8000 zones in radius. We measure an adiabatic torque excess  $\Gamma_1 = -1.14 \cdot 10^{-11} M_* \Omega_p^2 r_p^2$ , by performing a run with similar characteristics and an isothermal equation of state. This allows us to predict the jump of angular velocity at the downstream separatrices by the use of Eq. (62). The results are depicted in Fig. 7, which shows the profile of perturbed azimuthal velocity in the rear and front of the planet, as well as the prediction of Eq. (62). We note that the jumps are not symmetric, although there is a good agreement between the theoretical prediction of the velocity jump on the one hand, and the average value of the rear and front velocity jumps on the other hand. One reason for that is that the perturbed pressure at the separatrices is not negligible compared to the perturbed pressure at the stagnation point. Another one is the asymmetry of the horseshoe region: both separatrices do not have same value of  $|(\Omega_+ + \Omega_-)/2 - \Omega_p|$ .

We note that for the run presented here, for which  $\mathcal{S} > 0$ , we have a negative torque excess, hence a negative perturbation of surface density in front of the planet, and a positive one behind the planet (Baruteau & Masset 2008). The fact that we have a positive perturbation of azimuthal velocity in front of the planet (dashed curve of Fig. 7) is compatible with an expansion of the material and consequently a decrease of surface density, because this perturbed velocity acts along with the Keplerian shear. Reciprocally, we have also a positive perturbation of velocity behind the planet, therefore opposed to the Keplerian shear, and compatible with a compression of material, hence an increase of the

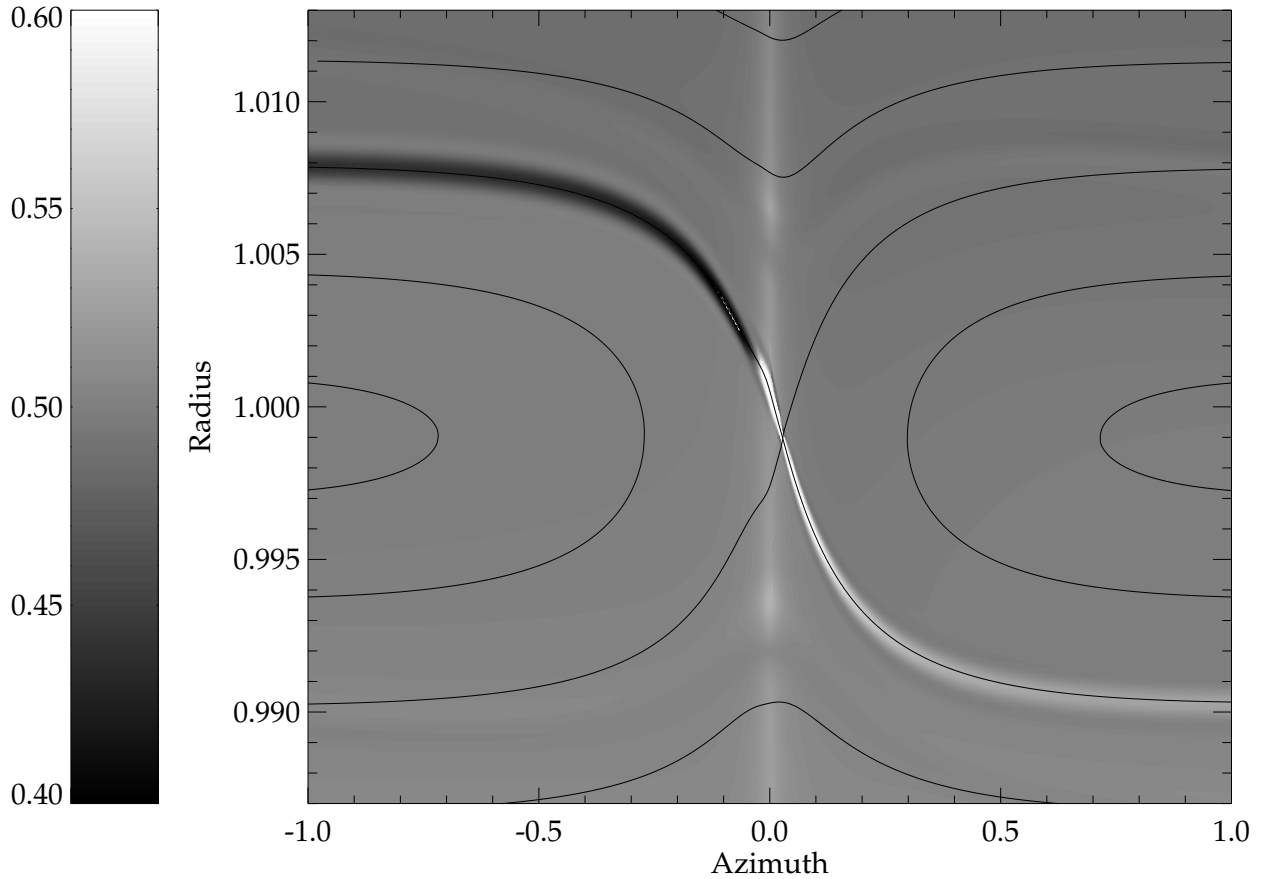


Fig. 6.— Vorticity field in the vicinity of an Earth-mass planet at  $t = 64$  orbits. The characteristics of the run are described in the text. The vorticity sheets are clearly apparent on the separatrices. Also, we note that the sign of the vorticity does not reverse at the stagnation point, but somewhere further on the downstream rear separatrix. The reason for this is that the perturbation of pressure is larger over the portion of the separatrix involved than at the stagnation point, as it crosses the wake. We also note that the vorticity is not singular on the upstream separatrices, which results from the fact that  $G$  is continuous across them.

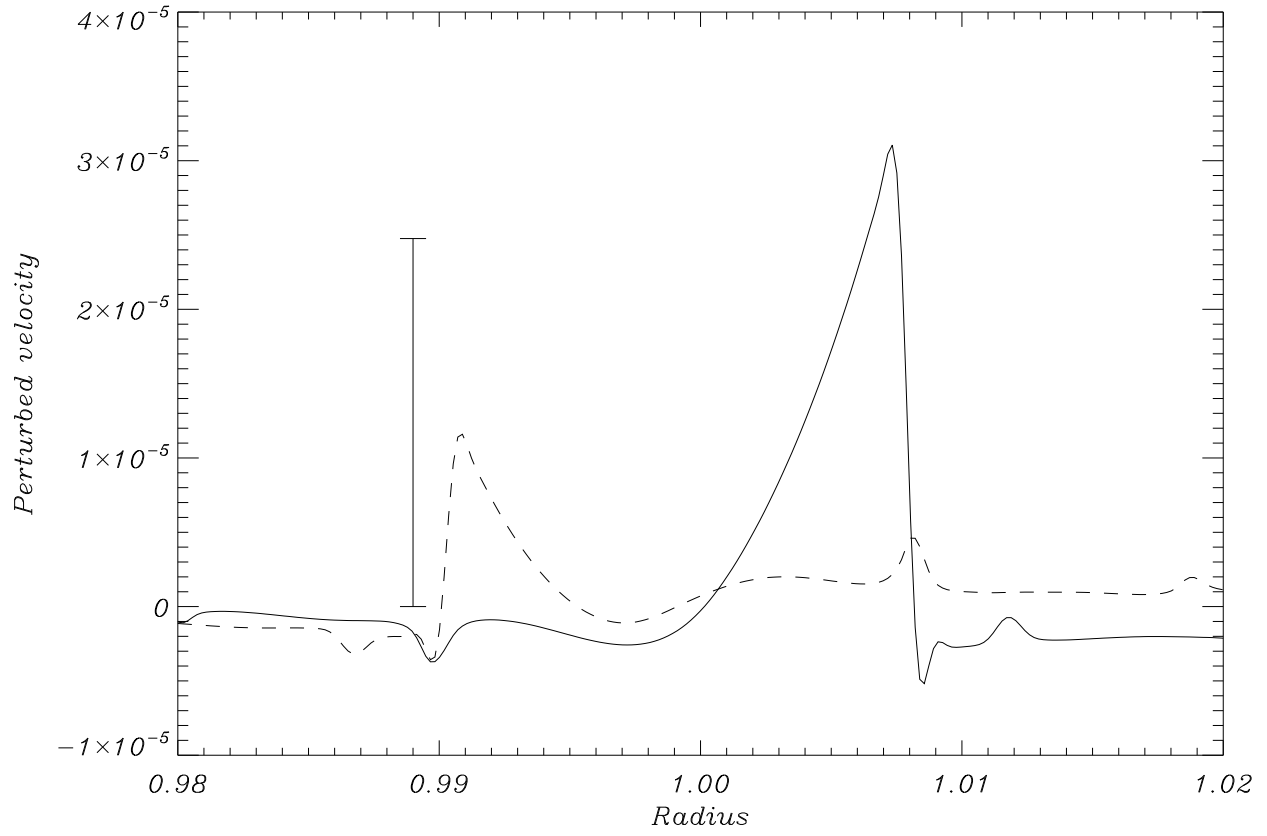


Fig. 7.— Perturbed azimuthal velocity at  $t = 64$  orbits, as a function of radius, at  $\phi = 1$  rad (dashed line) and at  $\phi = -1$  rad (solid line). The vertical bar at the left shows the expected magnitude of the velocity jump, obtained from a measure of the torque excess using Eq. (59), and using the result in Eq. (62).

surface density.

Finally, we mention that the vortensity is ill-defined at the separatrices. Whereas the vorticity is definable, the integral of its singular part yielding the azimuthal velocity jump, the vortensity would appear, on the separatrix, as the ratio of a singularity (that of the vorticity) by a non-continuous function (owing to the contact discontinuity, the surface density undergoes a jump at the separatrix), which is mathematically undefined. On the contrary, in the locally isothermal case (see paper I), the surface density field is continuous and the vortensity is defined everywhere.

## 5.2. Production of vortensity

On the contrary to a barotropic situation, for which the vortensity is necessarily conserved along the streamlines (Lovelace et al. 1999), some thermodynamical driving of the vortensity may occur during the horseshoe U-turns. We also note that far from these U-turns, the vortensity is conserved again, since all quantities depend only on  $r$ , hence the pressure and density gradients are both radial, hence aligned.

Using Eq. (23) and (27), we are left with:

$$\left. \frac{\Sigma}{\omega} \right|_d = \left. \frac{\Sigma}{\omega} \right|_u \left( 1 - \delta T \frac{\partial_r S_0}{4ABx} \right). \quad (63)$$

We comment that we have used the relationship  $\partial_S G = -\partial_r S_0 / (4ABx)$  to obtain Eq. (63). The bracket of this equation corresponds indeed to material downstream of a horseshoe U-turn. During a U-turn,  $\partial_G S$  is conserved, while  $x$ , to lowest order, reverses its sign, and Eq. (23) has been written for the unperturbed disk, that is to say upstream of horseshoe U-turns. The perturbation of temperature, within the horseshoe region, can be easily worked out assuming the conservation of entropy and an unperturbed pressure. This yields

(Baruteau & Masset 2008):

$$\delta T = -2T_0 \mathcal{S} \frac{x}{r_p}. \quad (64)$$

Using Eqs. (63) and (64) we get the production of vortensity during a U-turn:

$$\delta \left( \frac{\Sigma}{\omega} \right) = \frac{\Sigma}{\omega} \Big|_d - \frac{\Sigma}{\omega} \Big|_u \approx \frac{\gamma T_0 \mathcal{S}^2}{2(\gamma - 1) A B r_p^2} \cdot \frac{\Sigma_0}{2B}. \quad (65)$$

We illustrate this in Fig. 8, which shows that there is a satisfactory agreement between the vortensity on the downstream side (here, outside, at the rear of the planet) and the vortensity predicted by Eq. (65). We also note in this figure how the vortensity near corotation differs from the expected value, both on the inside and on the outside. On the outside, this is expected because the material very close to corotation did not have sufficient time to perform a horseshoe U-turn. On the inside, for  $0.996 \leq r \leq 0.999$ , libration on tadpole streamlines brings vortensity from the outside, thereby yielding a perturbation of vortensity in the upstream region. More generally, the fact that streamlines are not exactly circular alters the initial profile of vortensity in this region. We also note the spike at the outer separatrix, resulting from the vorticity sheet presented in section 5.1, where we also pointed out that, formally, the vortensity is ill-defined on the downstream separatrices.

We can make the following observations regarding Eq. (65):

- There is always a positive production of vortensity during the U-turns (hence a decrease of  $\Sigma/\omega$ ), regardless of the sign of  $\mathcal{S}$ , and regardless of the location (at the rear or in front of the planet).
- The production of vortensity is independent of the planet mass, and it occurs uniformly all over the downstream sides of the horseshoe region. While wider horseshoe U-turns bring the material closer to the planet, where the driving of vortensity is more efficient because the gradients of pressure and density are larger, they are performed faster than the more narrow U-turns, which occur further away

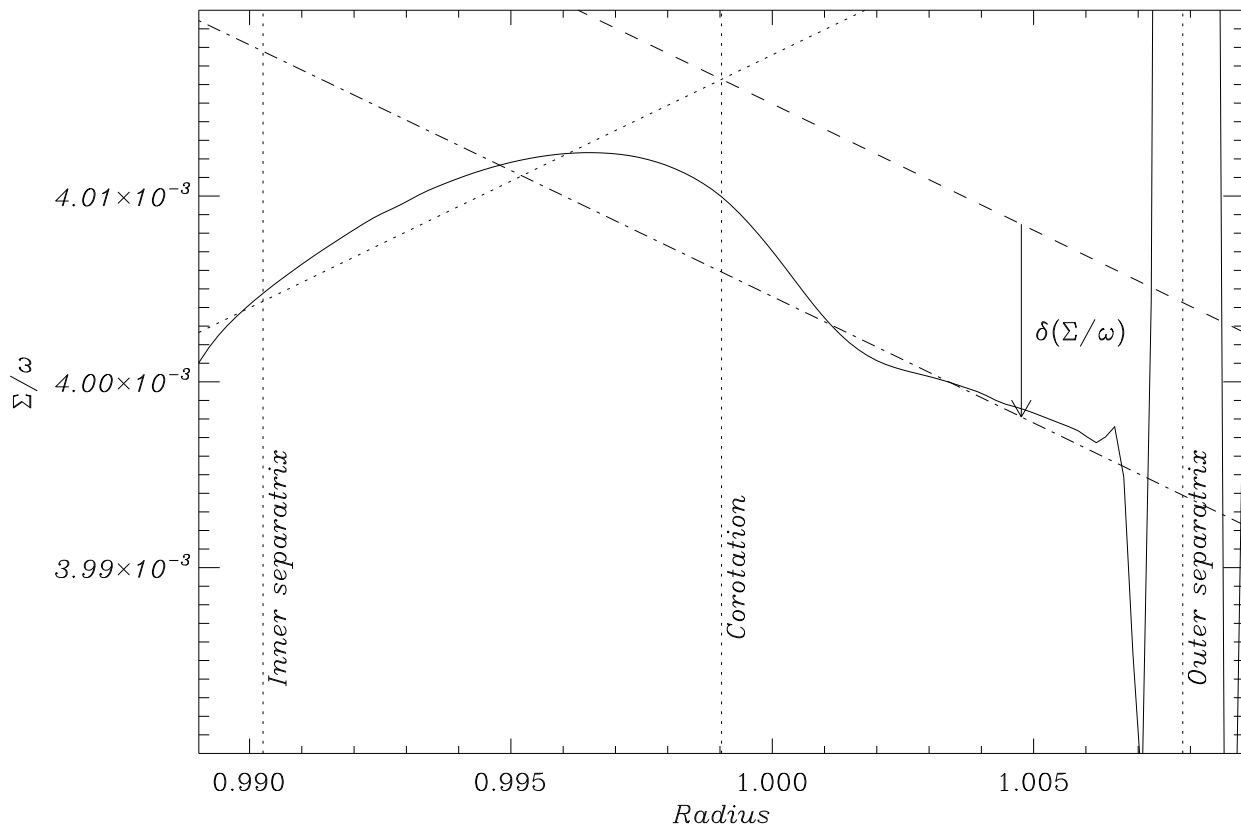


Fig. 8.— Radial profile of  $\Sigma/\omega$  at  $t = 48$  orbits and  $\phi = -1$  rad (solid line). The tilted dotted line shows the initial, unperturbed profile, while the tilted dashed line shows this profile symmetrized with respect to the corotation radius. It is therefore this profile that one would expect if vortensity were conserved. If one takes into account the production of vortensity given by Eq. (65), one obtains the dot-dashed line, which is in correct agreement with the observed profile.

from the planet. Eq. (65) shows that both effects cancel out, resulting in a flat profile of vortensity perturbation.

- If we translate the production of vortensity into a perturbation of density, assuming an unperturbed velocity field, then this perturbation has same sign on both sides of the planet. This is compatible with the fact that the bulk term of the horseshoe drag, i.e. the first term of Eq. (37), is the same as in a barotropic situation. The weak thermodynamical driving of vortensity observed within the horseshoe region has therefore no impact on the torque.
- The increase of vortensity after the first horseshoe U-turn is followed by a decrease of same magnitude at the following U-turn (in the idealized, inviscid situation considered here). This can be seen from Eq. (27), in which we revert the  $d$  and  $u$  indexes. The vortensity of a given fluid element therefore oscillates between its initial upstream value and its subsequent downstream value, and it does not undergo any drift on the long term.

### 5.3. Pressure disturbances

In this section we wish to determine the shape and amplitude of the pressure disturbances which arise in the coorbital region as the result of the horseshoe dynamics. In paper I, we have seen that the perturbation of vortensity was entirely accounted for by evanescent waves, so that the density or pressure response in the coorbital region was smoothed over a length-scale  $H$ . Here, we expect that the perturbation will be split into a localized part, which ends at the contact discontinuity at the separatrix, and a smooth part, corresponding to the launch of evanescent waves.

Far from the planet, we assume purely circular motion, hence we can describe the

disk's perturbed state with the perturbed azimuthal velocity  $\delta v_\phi(x)$ , the perturbed surface density  $\delta\Sigma(x)$ , and the perturbed pressure  $\delta P(x)$ . We search the relationship between this set of perturbed functions, and the perturbations of vortensity  $\delta w(x)$  and entropy  $\delta s(x)$ . We note that  $x$  has an arbitrary sign for the rest of this section. If we consider a radial profile in front of the planet, where the downstream separatrix lies inside of corotation, then  $x_s$  is meant to be a negative quantity.

Using Eq. (12), the disk's rotational equilibrium yields:

$$-2\Omega\delta v_\phi + \frac{\partial_x \delta P}{\Sigma_0} + \frac{\partial_x p_0}{\Sigma_0} \frac{\delta\Sigma}{\Sigma_0} = 0 \quad (66)$$

Anticipating on what follows, we note that while the radial derivative of an unperturbed quantity  $\xi_0$  is of order  $\xi_0/r$ , the radial derivative of a perturbed quantity  $\delta\xi$  is of order  $\delta\xi/H$ . The second term of Eq. (66) is therefore  $r/H$  times larger than the third one. This equation can therefore be simplified as:

$$-2\Omega_0\delta v_\phi + \frac{\partial_x \delta P}{\Sigma_0} = 0 \quad (67)$$

Denoting  $l = \Sigma/\omega$  the inverse of the vortensity, we can write:

$$\delta l = \frac{\delta\Sigma}{\omega_0} - \frac{\Sigma_0}{\omega_0^2} \partial_x \delta v_\phi, \quad (68)$$

while the perturbation of entropy reads:

$$\delta s = \frac{\delta P}{\Sigma_0^\gamma} - \frac{\gamma s_0}{\Sigma_0} \delta\Sigma. \quad (69)$$

Deriving Eq. (67) with respect to  $x$ , keeping only the derivatives of rapidly varying terms, i.e. the perturbations, and using Eqs. (68) and (69) so as to keep only the variable  $\delta P$ , we obtain the following differential equation:

$$\delta P - \frac{c_s^2}{\kappa^2} \partial_{x^2}^2 \delta P = c_s^2 \Sigma_0 \frac{\delta u}{u_0}, \quad (70)$$

where  $\kappa = (2\Omega_0\omega_0)^{1/2}$  is the epicyclic frequency,  $u = s^{1/\gamma}l$ , and where we recall that  $c_s$  is the adiabatic speed of sound (see section 2.1). The general solution of Eq. (70) is the convolution product of its right hand side by the Green's kernel  $K(x)$ , which is the solution of:

$$\delta P - \frac{c_s^2}{\kappa^2} \partial_{x^2}^2 \delta P = \delta(x), \quad (71)$$

and whose expression is:

$$K(x) = (2\gamma^{1/2}H)^{-1} e^{-|x|/(\gamma^{1/2}H)}, \quad (72)$$

where we have specialized to the Keplerian case, for which  $H \equiv c_s^{\text{iso}}/\Omega = c_s/(\gamma^{1/2}\kappa)$ . This kernel represents the pressure response to a singular perturbation of  $u$  at  $x = 0$ , of weight  $\int u(x)dx = u_0/(c_s^2\Sigma_0)$ . We note that  $K(x)$  has a unitary weight:

$$\int_{-\infty}^{+\infty} K(x)dx = 1. \quad (73)$$

Once the pressure response is known, one can infer the density response from Eq. (69):

$$\delta\Sigma = \frac{\Sigma_0}{\gamma} \left( \frac{\delta P}{P_0} - \frac{\delta s}{s_0} \right). \quad (74)$$

Denoting  $\delta\Sigma_d = \delta P/c_s^2$  and  $\delta\Sigma_l = -\Sigma_0\delta s/(\gamma s_0)$ , we have:

$$\delta\Sigma = \delta\Sigma_d + \delta\Sigma_l. \quad (75)$$

In Eq. (75), the subscript  $d$  stands for *diffuse*, since this component of the surface density scales with the perturbed pressure, which is smoothed over a length-scale  $H$  by the action of evanescent waves, as it involves the convolution of an arbitrary function by the kernel  $K$  defined at Eq. (72). Similarly, the subscript  $l$  stands for *localized*, since this component of the surface density scales with the perturbation of entropy, which is advected by the flow, and remains localized within the horseshoe region.

Since  $\delta P$  is the convolution product of  $K$  by  $c_s^2\Sigma_0\delta u/u$ , we have:

$$\delta\Sigma_d = K * \Sigma_0 \frac{\delta u}{u_0}, \quad (76)$$

where  $*$  denotes the convolution product. Similarly, we have:

$$\delta\Sigma_l = -\frac{\Sigma_0}{\gamma} \frac{\delta s}{s_0}. \quad (77)$$

The expression of the entropy perturbation is straightforward, as the latter is simply advected by the horseshoe dynamics. Since  $s \propto r^{\gamma\mathcal{S}}$ , we have  $\delta s/s_0 = -2\gamma\mathcal{S}x/r_p$ , hence (Baruteau & Masset 2008):

$$\delta\Sigma_l = 2\Sigma_0\mathcal{S}x/r_p. \quad (78)$$

The expression of the perturbation of  $u$  involves three components: the singular contribution of the vorticity sheet at the separatrix, the advection of the vortensity and entropy by the horseshoe dynamics, and the production of vortensity given by Eq. (65). We have mentioned in section 5.1 that the vortensity is ill-defined on the downstream separatrices, since the surface density is discontinuous there. Nevertheless, the jumps of surface density are of order  $x_s/a$ , hence to lowest order the vortensity can be estimated to be  $\Delta v\delta(x - x_s)/\Sigma_0$  at the separatrices. We can therefore estimate the perturbation in  $u$ :

$$\frac{\delta u}{u_0} = -\frac{\Delta v\delta(x - x_s)}{\omega_0} - \frac{2x}{r_p}(\mathcal{S} + \mathcal{V}) + \frac{\delta l_{\text{prod}}}{l_0}, \quad (79)$$

where we have used the fact that  $u \propto r^{\mathcal{S}+\mathcal{V}}$ , and where, using Eq. (65):

$$\frac{\delta l_{\text{prod}}}{l_0} = \frac{\gamma T_0 \mathcal{S}^2}{2(\gamma - 1)ABr_p^2}. \quad (80)$$

For the sake of brevity, in what follows, we will keep the notation  $\delta l_{\text{prod}}$ , remembering that it corresponds to a uniform production of vortensity that scales with  $\mathcal{S}^2$ , and which has same sign on both sides of the planet. The perturbation of density finally reads:

$$\delta\Sigma = K * \left[ -l_0\Delta v\delta(x - x_s) - \frac{2x}{r_p}\Sigma_0(\mathcal{S} + \mathcal{V}) + \frac{\Sigma_0\delta l_{\text{prod}}}{l_0} \right] + \frac{2x}{r_p}\Sigma_0\mathcal{S}. \quad (81)$$

Eq. (81) features two kinds of terms:

- bulk terms (second to fourth term), which are defined for  $0 \leq x \leq x_s$ , prior to a possible convolution by  $K$ ;

- an edge term (the first one), which is defined at  $x = x_s$ , prior to the convolution by  $K$ .

We better understand why the bulk of the horseshoe drag has the same expression as in the barotropic case. The convolution by  $K$ , which describes the spread of disturbances by evanescent waves, does not change the linear mass ( $\int_x \delta\Sigma(x)dx$ ) of the perturbation, since  $K$  has a unit weight. Therefore, the torque exerted on the planet by the diffuse and localized stripes of perturbed density is the same as if all the disturbances remained localized, i.e. as if we omitted the convolution product in Eq. (81). If we discard the singularity, which corresponds to the edge term (and, as we shall see, to the adiabatic torque excess), and the production of vortensity, which has same sign on both sides of the planet and does not affect the torque, we are left with the middle term of the bracket of Eq. (81), and the trailing, localized term, which simplify as:

$$\delta\Sigma = -\frac{2x}{r_p}\Sigma_0\mathcal{V}, \quad (82)$$

exactly as in the barotropic case, prior to the convolution by the Green's kernel (see paper I). These properties are schematically depicted in Fig. 9.

This first term of Eq. (81) corresponds to a single evanescent wave excited at the separatrix. It is the perturbed density associated with this wave that exerts the adiabatic torque excess, since it is the only component that scales with the entropy gradient, owing to the simplification mentioned above. This is in agreement with Eq. (37), which shows that the torque excess comes from an edge effect rather than a bulk effect, since it relies on a minute difference between the limit of the integration domain between the rear and front sides. We can check from Eq. (62) that this edge term has correct sign. Since the perturbed density associated to this wave has a sign opposite of  $\Delta v$ , the perturbed density has same sign as  $\Gamma_1$  in front of the planet, and an opposite sign behind the planet, as expected.

A consequence of these properties is that, contrary to early expectations, it is not the localized component of the surface density that exerts the torque excess. The latter does

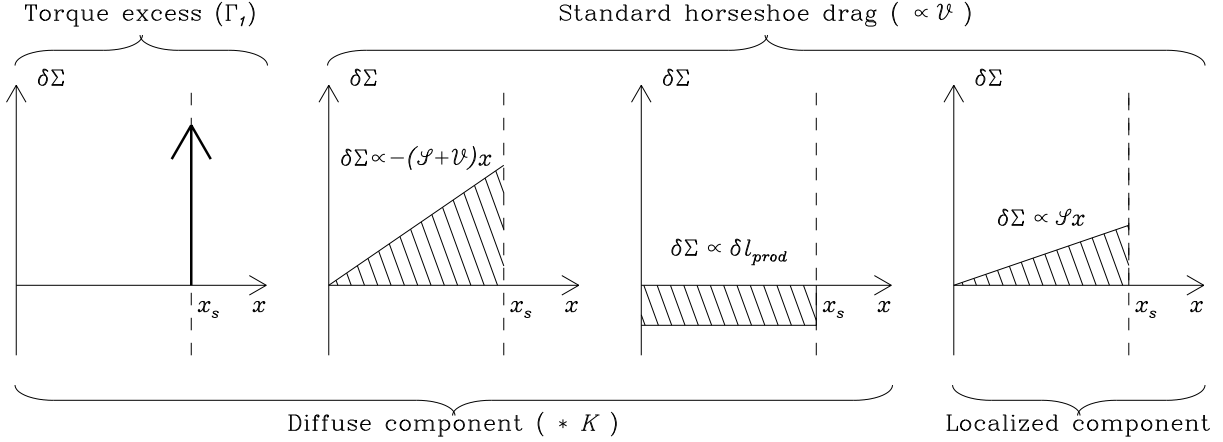


Fig. 9.— Schematic representation of the different terms of Eq. (81), in their order of appearance in the right hand side. The vertical arrow on the left plot represents the singularity at the separatrix. The first three terms represent the pressure supported density response, which is obtained by a convolution of the response depicted by the evanescent wave kernel of Eq. (72). The last term remains confined to the horseshoe region and is associated to the entropy wave. The terms are here depicted for  $x > 0$ , i.e. behind the planet. In front of the planet, they would have an opposite sign, except the third term, corresponding to the production of vortensity, which would remain negative and has therefore no impact on the torque.

exert a torque on the planet, which can be estimated either by means of a partial horseshoe drag calculations (Baruteau & Masset 2008), or by direct summation (Paardekooper & Papaloizou 2008). It is found to have same sign as the excess, and same order of magnitude in usual setups. Nevertheless, this partial torque has to be added to the torque exerted by the diffuse component which scales as  $\mathcal{S} + \mathcal{V}$ , and the result is a corotation torque that scales only with the vortensity gradient. This can be expected on general grounds. The splitting of the perturbation into a localized component (an entropy wave) and pressure supported waves is very similar to the procedure used by numericists who use characteristic tracing to predict Riemann states, except that here the pressure supported waves are evanescent instead of propagative. The entropy perturbation regulates how much of the perturbation goes into the entropy wave, but it is the vortensity perturbation that dictates the total amount of mass perturbation, and it is therefore logical that the bulk of the corotation torque scales with the vortensity gradient.

Owing to the simplicity of the functions involved in the convolution product, it is possible to write explicitly the expression of the pressure perturbation. This is done in appendix A. We show in Fig. 10 that the resulting expression, given by Eq. (A5), satisfactorily reproduces the perturbations of pressure observed in numerical simulations. Namely, we transform the profile of perturbed pressure from a numerical simulation as follows, in order to filter out the term arising from the production of vortensity, which is poorly reproduced by a rectangular function, as it has been shown in Fig. 8:

$$\delta P_{\text{sym}}(x) = \frac{1}{2}[\delta P(\phi = 2\pi - 1, x) - \delta P(\phi = 1, -x)] \quad (83)$$

We then evaluate the theoretical expression of the perturbed pressure given by Eq. (A5), in which we use for  $\Gamma_1$  the estimate provided by Eq. (59) (corresponding to the thick dashed curve of Fig. 5), and for  $x_s$  the arithmetic mean of  $x_F^d$  and  $x_R^d$ , determined by a streamline analysis. Owing to the symmetrization performed in Eq. (83), we discard the term in  $\delta l_{\text{prod}}$

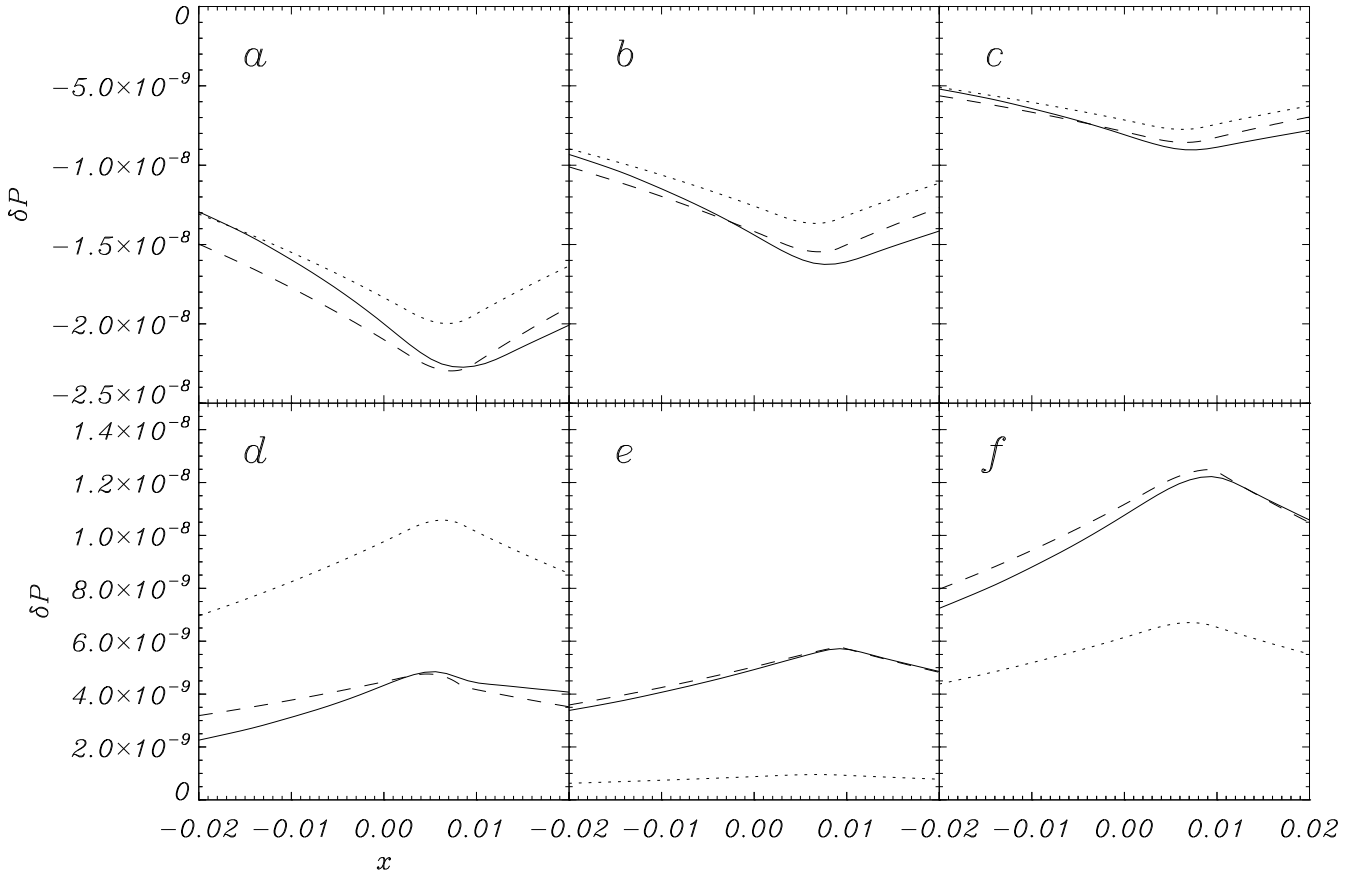


Fig. 10.— Profile of pressure perturbation for the calculations  $EA_0$  (a),  $EA_8$  (b),  $EA_{16}$  (c),  $EA_{24}$  (d),  $EA_{32}$  (e) and  $EA_{40}$  (f). The solid line shows the profile observed in numerical simulations, evaluated using Eq. (83), and the dashed line shows the result of Eq. (A5). The dotted line shows the partial result of Eq. (A5), in which we omit the first term, which corresponds to the isolated evanescent wave at the separatrix corresponding to the torque excess. The results of the plot *d* have been multiplied by  $-3$ , in order to make it more legible. This case corresponds to an approximate cancellation of the pressure term stemming from the  $\mathcal{S} + \mathcal{V}$  term and of the single evanescent wave excited at the separatrix. The case of the plot *e* is also of interest: for this calculation,  $\mathcal{V} + \mathcal{S} \approx 0$ , as can be seen from the dotted line, hence the pressure perturbation almost exclusively consists of the single evanescent wave excited at the separatrix, which is responsible for the torque excess.

in Eq. (A5). The correct agreement between the observed and predicted pressure profile indirectly confirms that it is indeed the single evanescent wave excited at the separatrix that is responsible for the torque excess. We also recover a feature noticeable in Fig. 5. While the plots  $a$  and  $f$  of Fig. 10 correspond to the same absolute value of the entropy gradient (namely  $8/7$ ), the single evanescent wave has a much larger amplitude in the case  $\mathcal{S} > 0$  (i.e. for the plot  $f$ ), almost of a factor of two, as can be seen from the distance between the dotted and dashed curves. This is compatible with the fact that, in Fig. 5, we found that the corrected torque excess, in absolute value, is almost a factor of two larger at  $\mathcal{S} = 8/7$  than at  $\mathcal{S} = -8/7$ .

## 6. Interpretation: an intrinsic asymmetry

We have seen in paper I how the excitation of evanescent pressure waves alters the width of the horseshoe region, in a different manner in front of the planet and behind the planet, so that it renders the horseshoe region asymmetric. This asymmetry, however, was found to have virtually no impact on the horseshoe drag, while the separatrices all shared the same value of the Bernoulli invariant. In the adiabatic case considered here, the evanescent waves launched downstream of the U-turns (see section 5.3) also alter the horseshoe width and render the horseshoe region asymmetric, but there is another source of asymmetry that preexists the launch of evanescent waves. Let us assume for a moment that the disk is composed of non-interacting test particles, so that there are no evanescent waves excited by the horseshoe motion, but let us also assume that the separatrices of the horseshoe region are given by the  $G_+$  and  $G_-$  values, as in an adiabatic disk (the expansion of  $G$  to lowest order in  $x$ , given by Eq. (19), is independent of the disk’s thermodynamics.) A different value for  $G_-$  and  $G_+$  implies a different upstream half width of the horseshoe region. Such a case is depicted in Fig. 11. The test particle  $A$ , which lies outside of the

separatrix, is circulating, and therefore mapped to  $A'$  by the flow. Similarly, the test particle  $B$  lies inside of the separatrix, and thus is librating. It is therefore mapped to  $B'$  by the horseshoe motion. There is therefore an over-density in the darker stripe in the bottom right quadrant of Fig. 11, as test particles of different origins merge into this stripe. Reciprocally, a void region appears at the downstream rear separatrix (the white stripe in the top left quadrant of Fig. 11). This region can neither be reached by the test particles executing horseshoe U-turns, as these are too narrow, nor can it be reached by test particles of the outer disk. The net effect of the asymmetry is that two stripes of perturbed surface density  $\pm\Sigma_0$  appear at the downstream separatrices, with a width

$$\delta x_s = \left| \frac{\Delta G}{\partial_r G} \right| = \left| \frac{\Delta G}{4ABx_s} \right| \quad (84)$$

The linear mass of these stripes is therefore, in absolute value:

$$\lambda = \Sigma_0 \left| \frac{\Delta G}{4ABx_s} \right| = \frac{\Sigma_0}{2B} |\Delta v| = l_0 |\Delta v|, \quad (85)$$

where we have used Eq. (62). This linear mass corresponds to the factor of the  $\delta$ -function in the bracket of Eq. (81). The torque due to the stripes can be evaluated as follows. The symmetric, barotropic case would be recovered if one sent the excess of surface density of the overdense stripe to the empty stripe, spending angular momentum for this purpose at the rate:

$$|\Gamma_1| = 4aBx_s \cdot |2Ax_s\Sigma_0\delta x_s|, \quad (86)$$

where the factor in absolute value represents the mass flow rate in the stripes. Using Eqs. (84) and (86), one recovers the expression of the torque excess, given by the last term of the right hand side of Eq. (37). In the case considered in Fig. 11, which has a wider horseshoe region at the front of the planet, one would have to give angular momentum to the material in excess in the front stripe, in order to recover a symmetric situation. Differently said, this implies that in the adiabatic situation the disk's material receives less

angular momentum than in the barotropic case, hence that there is a negative torque excess on the disk, and a positive torque excess on the planet, by virtue of the action and reaction law. This can also be deduced simply from the distribution of perturbed density, since there is a positive perturbed density in front of the planet and a negative one behind the planet.

In a disk with pressure, narrow stripes of surface density are spread radially by the excitation of evanescent waves, which are not easily detectable (see section 5.3). They leave however an imprint on the flow in the form of vorticity sheets. These are the most tangible perturbations of the flow associated to the torque excess.

One can also understand that the torque excess due to these stripes can in principle be extremely high. While the surface density perturbation in the barotropic case typically amounts to  $O(\Sigma_0 x_s/a)$  (prior to the convolution by the evanescent wave kernel), the stripes contemplated here correspond to a perturbation of surface density that is  $\pm\Sigma_0$ . If the asymmetry becomes large enough to represent a sizable fraction of  $x_s$ , the linear mass of the perturbation associated to the excess supersedes the linear mass of the vortensity related perturbation by a factor  $O(a/x_s)$ , that is to say typically by two orders of magnitude, for the situations considered here.

Further insight into the origin of the asymmetry can be gained by considering, for the sake of simplicity, an idealized situation in which the stagnation point lies at  $\phi = 0$ , i.e. at the maximum of the perturbed pressure. We can then evaluate, in order of magnitude, how the torque acting on a fluid element moving along an upstream separatrix differs from the barotropic case, and infer from this how the separatrix should be shifted. This situation is depicted in Fig. 12. For the sake of definiteness we assume that there is a negative radial entropy gradient.

The perturbation of density associated to the advection of entropy in the adiabatic case (see Baruteau & Masset 2008) enhances or diminishes the specific pressure torque  $-\nabla P/\Sigma$ .

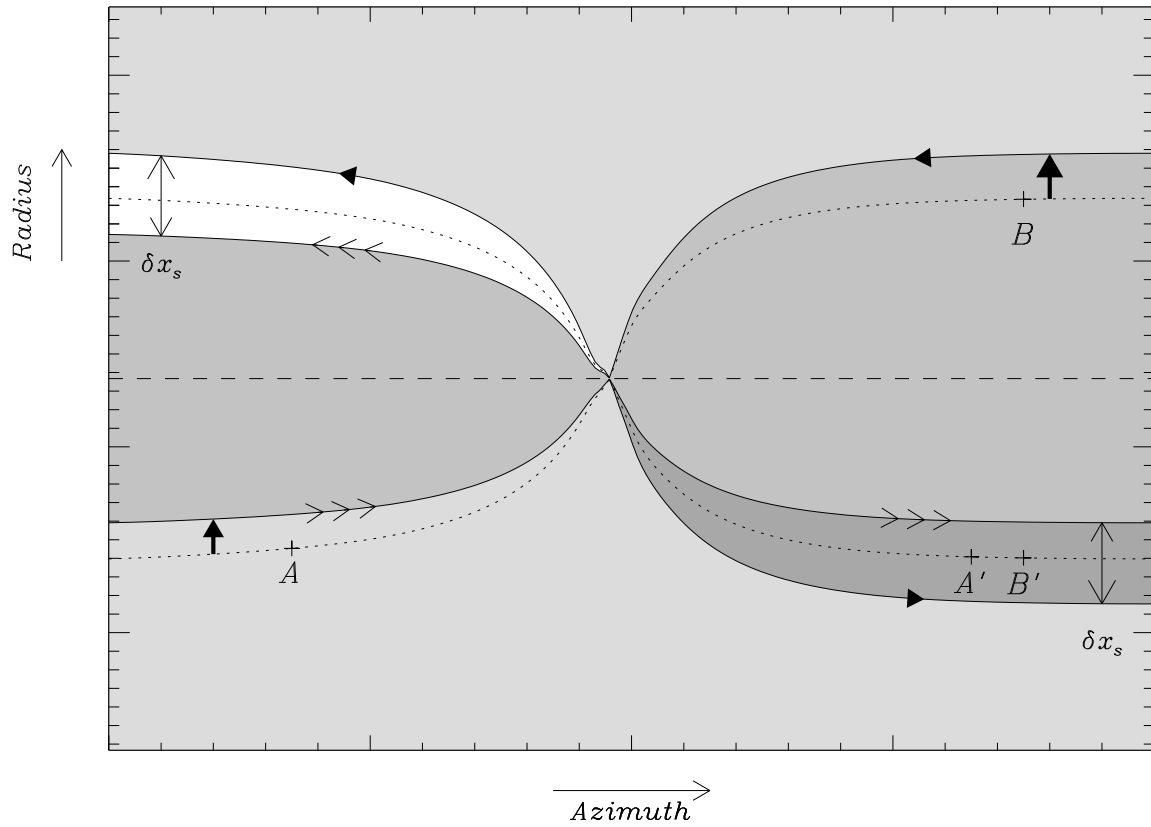


Fig. 11.— Schematic representation of an asymmetric horseshoe region. The dotted lines represent the symmetric separatrices of a barotropic situation. With respect to this case, the rear separatrix is shifted towards corotation, while the front separatrix is shifted away from corotation. The width  $\delta x_s$  of the stripes has been exaggerated to improve legibility.

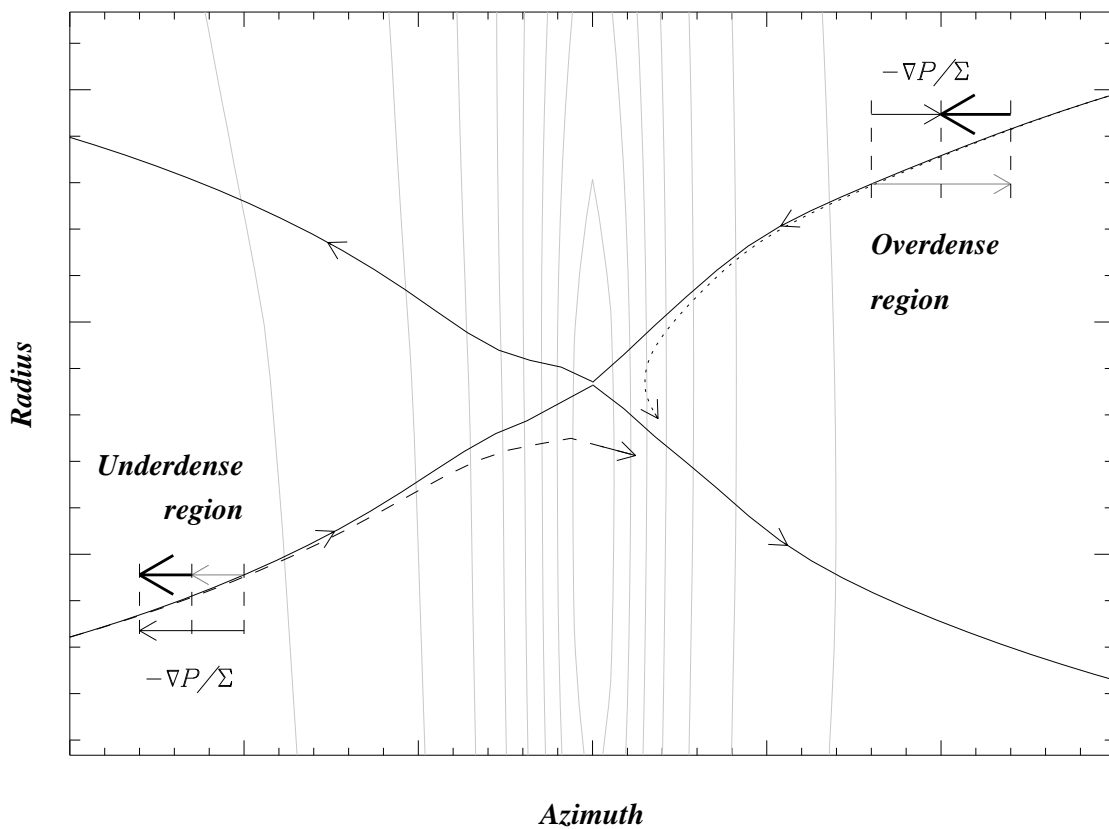


Fig. 12.— Schematic view of the action of the pressure gradient in an idealized case. The grey contours represent the perturbed pressure. The solid lines depict the separatrices of a barotropic case. The grey thin arrows represent  $-\nabla P/\Sigma$  in the barotropic case, and the black thin arrows the same quantity in the adiabatic case, the difference arising essentially from the variations of  $\Sigma$  between both cases. The thick arrows represent the excess of  $-\nabla P/\Sigma$ , which is negative on both sides of the planet. The fluid particle initially located on the rear upstream separatrix of the barotropic case therefore becomes circulating, as depicted by the dashed streamline. Similarly, the fluid parcel of the front separatrix loses more angular momentum than it would lose on the barotropic separatrix, hence the streamline associated to it is librating, as indicated by the dotted streamline.

As can be seen in Fig. 12, a consequence of this change is to render the horseshoe region asymmetric: the rear part shrinks, whereas the front part expands. A coarse estimate of the variation of the width of the horseshoe region can be given as follows. A fluid element on a separatrix, when it reaches the azimuth of the stagnation point, has received exactly the amount  $J$  of angular momentum necessary to bring it to the stagnation point (by definition of the separatrix):

$$J = \int_{-\infty}^{t_s} \left( -\partial_\phi \Phi - \frac{\partial_\phi P}{\Sigma} \right) dt = 2Br_p x_s, \quad (87)$$

where  $t_s$  is the date at which the fluid element reaches the stagnation point. Assuming the fluid element to have at any instant in time the azimuthal velocity of the unperturbed Keplerian shear, we can write:

$$J = \int_{-\infty}^{\phi_s} \frac{r_p}{2Ax} \left( \partial_\phi \Phi + \frac{\partial_\phi P}{\Sigma} \right) dt = 2Br_p x_s. \quad (88)$$

A rough estimate of how  $x_s$  varies when the pressure term is modified can be obtained by taking  $x$  out the integral in Eq. (88), assuming that it is everywhere equal to  $x_s$ .

At this level of approximation, the perturbation of the pressure term can be written as  $\sim (\partial_\phi P/\Sigma_0)(2\mathcal{S}x_s/a)$ . We are then left with:

$$\left( \int_{-\infty}^{\phi_s} \frac{\partial_\phi P}{\Sigma_0} d\phi \right) \cdot (2\mathcal{S}x_s/a) \sim 2ABx_s \delta x_s, \quad (89)$$

which can be recast as:

$$\delta x_s \sim \frac{p_s \mathcal{S}}{2ABa\Sigma_0}. \quad (90)$$

We note that we obtain the same expression for the variation of the horseshoe width using Eqs. (41), (50), (54) and (84), within a factor of order unity (the value  $\delta x_s$  obtained above just refers to the variation of the width of one side of the horseshoe region, whereas the expression worked out earlier in this section and depicted by the thin double arrows in Fig. 11 corresponds to adding the width variation of the front and rear sides.)

This order of magnitude estimate allows to identify the origin of the horseshoe asymmetry, and allows to understand why the adiabatic torque excess scales with the

perturbation of pressure at the stagnation point ( $p_s$ ), at least in the regime of small planetary masses (for which  $p_s \ll P_0$ .) We finally note that, while this order of magnitude was obtained in the simplified case of a stagnation point located at the maximum of perturbed pressure, it still holds when the stagnation point is azimuthally shifted, as in real situations. A more refined treatment of the dynamics of a fluid element moving along the separatrices would have exhibited its Bernoulli invariant, and it would have led to an exact relationship such as Eq. (44), which is equivalent to Eq. (88). This relationship shows that the width of the horseshoe region depends exclusively of the flow properties of the stagnation point, independently of the location of the latter and of the path followed by the fluid elements.

## 7. A suitable torque expression

The torque expression of Eq. (55) involves the planetary potential at the stagnation point, as well as the distance of the upstream separatrices to corotation. As such, it is not well suited for torque estimates, and needs further transformation.

We have seen in section 4.2 that the half width of the horseshoe region has a complex dependence on the disk’s and planet’s parameters in the adiabatic case. In particular, at large values of  $|\mathcal{S}|$ , the horseshoe region is wider than in the barotropic case, which boosts the vortensity related corotation torque. The global torque excess is therefore the sum of two non-trivial individual excesses: the one related to the gradient of entropy, which has been studied in depth in the preceding sections, and the one related to the boost of the vortensity related corotation torque. We note however in Fig. 5 that the global excess, which corresponds to the dotted curve, has an almost linear dependence on the entropy gradient. Our aim is therefore to exhibit a separable form of the torque excess that involves the product of  $\mathcal{S}$  by a function of  $\hat{\epsilon}$ . This expression aims at describing the global torque

excess, therefore accounting for the whole difference between the adiabatic and barotropic case. For this purpose we can simply use the data of the series  $SA_i$ , which has a null vortensity gradient and for which the adiabatic torque excess accounts for the whole excess. We then rescale the function obtained to get the excess at any entropy gradient.

### 7.1. Scaling of the torque excess

We first establish the scaling of the torque excess as a function of the disk's and planet's parameters. Eq. (55) shows that the torque excess involves the half width of the horseshoe region, and the potential at the stagnation point. In order to remain in the framework of a separable expression, we neglect the dependence of  $x_s$  on the entropy gradient, mentioned in section 4.2, and we use the barotropic approximation (i.e. for  $\mathcal{S} = 0$ ) to infer the half width. Using Eq. (57), we obtain:

$$x_s^{\text{adi}} = \frac{C(\hat{\epsilon})}{\gamma^{1/4}} a \sqrt{\frac{q}{h}}, \quad (91)$$

where  $C(\hat{\epsilon})$  is a dimensionless constant that depends on the softening length (Paardekooper & Papaloizou 2009b). Examination of Fig. 3 shows that this approximation leads to errors of at most  $\sim 30\%$ . We check in what follows that the potential at the stagnation point can also be considered as essentially independent of the entropy gradient.

#### 7.1.1. Potential at the stagnation point

Evaluating the planetary potential at the stagnation point requires to know the location of this point. Writing the Euler equations in steady state, in a system of units in which the unit of length is  $H = c_s/\Omega$ , one can realize that, as long as the planet is deeply embedded (i.e.  $aq^{1/3} \ll H$ ), the azimuth of the stagnation point (which lies almost on corotation) has to scale as  $hf(\hat{\epsilon})$ , where  $f$  is a function that we shall determine and  $\hat{\epsilon} = \epsilon/H$

is a dimensionless value of the softening length. We have therefore:

$$\Phi_p^s = -\frac{GM_p}{H[f(\hat{\epsilon})^2 + \hat{\epsilon}^2]^{1/2}}. \quad (92)$$

Fig. 13 shows the location of the stagnation point as a function of  $\hat{\epsilon}$  in an adiabatic flow with  $\gamma = 1.4$ , obtained from the series of numerical simulations  $\text{EA}_{0 \leq i \leq 20}$  (see section 4.1), and a similar series with a different entropy gradient. Under  $\hat{\epsilon} \simeq 1.0$ , the distance of the stagnation point to the planet is larger than the softening length, and the denominator of Eq. (92) is dominated by the function  $f(\hat{\epsilon})$ , which is found to hardly depend on  $\mathcal{S}$ , as both series essentially coincide for  $\hat{\epsilon} < 1.0$ . Reciprocally, for  $\hat{\epsilon} > 1.0$ , the stagnation point lies within a softening length from the planet, and the potential at the stagnation point approximately scales as  $\hat{\epsilon}^{-1}$ , and is therefore also independent of the entropy gradient.

### 7.1.2. General expression of the torque excess

Using Eqs. (55), (91) and (92), we obtain:

$$\Gamma_1 = -A(\hat{\epsilon})\mathcal{S}\Gamma_0, \quad (93)$$

where  $\Gamma_0 = \Sigma_0 \Omega_p^2 q^2 a^4 / h^2$ , and where:

$$A(\hat{\epsilon}) = \frac{4C^2(\hat{\epsilon})}{\sqrt{1.4}} \left[ \frac{1}{\sqrt{f(\hat{\epsilon})^2 + \hat{\epsilon}^2}} - \frac{3}{8} \frac{C^2(\hat{\epsilon})}{\sqrt{1.4}} \right], \quad (94)$$

where we have specialized to the Keplerian case ( $A = -3\Omega/4$ ,  $B = \Omega/4$ ). Note that we explicitly restrict ourselves to the case  $\gamma = 1.4$ . Although Eq. (91) applies for arbitrary values of  $\gamma$ , the azimuth of the stagnation point, considered in section 7.1.1, may depend on the adiabatic index. Keeping an explicit dependence in  $\gamma$  in Eq. (94) could therefore be misleading. The adiabatic torque excess, given by Eq. (93), has a scaling similar to the barotropic corotation torque or the differential Lindblad torque (Tanaka et al. 2002). The

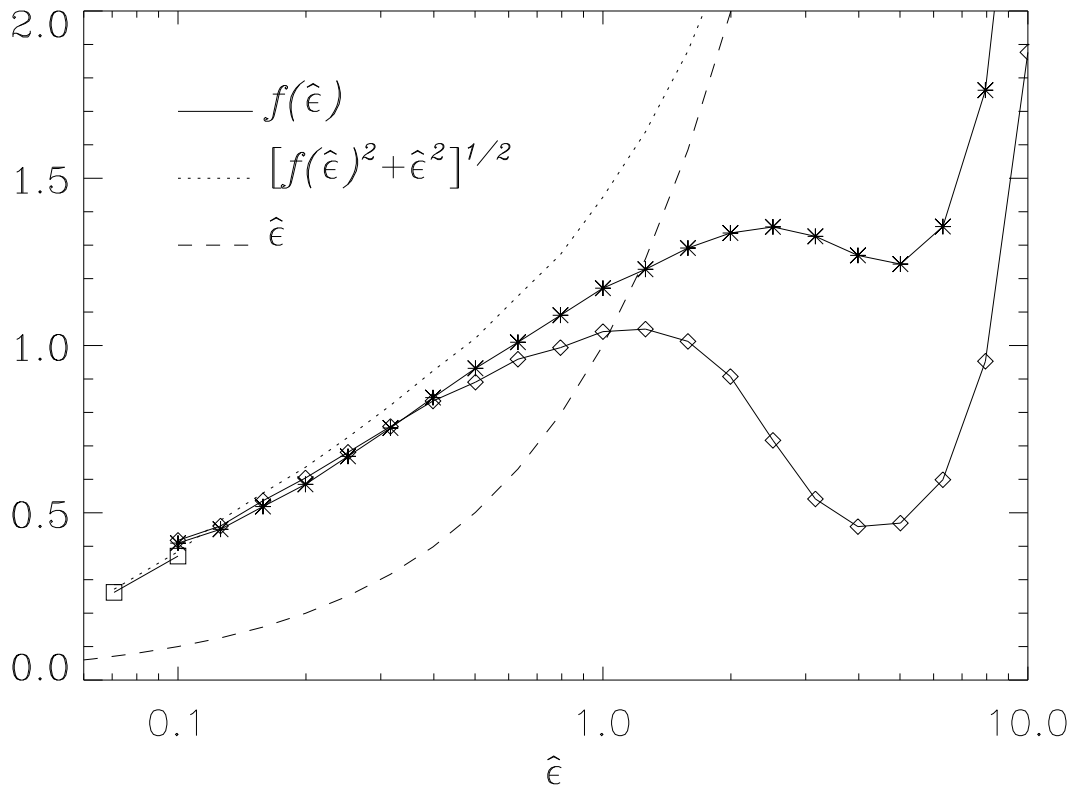


Fig. 13.— Location of the stagnation point as a function of the softening length, measured at  $t = 40$  orbits. Diamonds show values obtained in the  $EA_{0 \leq i \leq 20}$  series. The two squares show values obtained for the same parameters as in the EA series, except that the resolution has been increased to  $2000 \times 2000$ . The stars show values obtained from a series similar to EA, except that it has a different entropy gradient:  $\mathcal{S} = +12/7$ . The dotted curve, which shows  $[f(\hat{\epsilon})^2 + \hat{\epsilon}^2]^{1/2}$ , has been obtained using the data provided by the EA series.

only differences with the barotropic corotation torque is that the excess scales with  $\mathcal{S}$  rather than  $\mathcal{V}$ , and that it involves a different dimensionless function of  $\hat{\epsilon}$ .

In order to determine this function, we use the series  $SA_i$ , as explained above. We restrict ourselves to the range  $0.1 \leq \hat{\epsilon} \leq 1$ . Values of  $\hat{\epsilon}$  larger than one are not relevant, whereas values smaller than 0.1 are difficult to study owing to the very high resolution required. As mentioned in section 4.3, the torque excess exhibits a dependence in  $\hat{\epsilon}^{-1}$  with a good approximation over the range of  $\hat{\epsilon}$  considered (a dependence partly due to the increase of  $x_s$  at small softening length, and partly due to the increase of the planetary potential at the stagnation point at small softening length). Fitting the torque excess over the range of  $\hat{\epsilon}$  considered, we obtain:

$$A(\hat{\epsilon}) \approx \frac{1.3}{\hat{\epsilon}}. \quad (95)$$

The expression of the torque excess is therefore:

$$\Gamma_1 = -\frac{1.3\mathcal{S}}{\hat{\epsilon}}\Sigma_0\Omega_p^2q^2a^4h^{-2}. \quad (96)$$

One can see in Figs. 4 and 5 that this expression (which is represented by the grey dashed line) is in good agreement with the global adiabatic excess. It is also in good agreement with the results of Baruteau & Masset (2008).

## 7.2. Considerations on the three-dimensional case

If one considers that a two-dimensional case with softening length  $\epsilon$  represents the layer at altitude  $z = \pm\epsilon$  of a three dimensional case (see e.g. Masset 2002), one can perform an integration of the torque over  $\epsilon$  in order to get an approximate value of the three dimensional torque. A layer comprised between altitude  $z$  and  $z + dz$  has a surface density  $(\Sigma_0/\sqrt{2\pi}H) \exp[-z^2/(2H^2)]dz$ , hence the three dimensional adiabatic torque excess should

be approximately given by:

$$\begin{aligned}\Gamma_{3D} &\approx -2 \int_0^{+\infty} \frac{\Sigma_0}{\sqrt{2\pi}H} \exp[-z^2/(2H^2)] A\left(\frac{z}{H}\right) \mathcal{S}\Omega_p^2 \left(\frac{q}{h}\right)^2 r_p^4 dz \\ &\approx -\sqrt{\frac{2}{\pi}} \mathcal{S}\Gamma_0 \int_0^{+\infty} e^{-\hat{\epsilon}^2/2} A(\hat{\epsilon}) d\hat{\epsilon}\end{aligned}\tag{97}$$

While this kind of calculation can be performed relatively easily for the vortensity related torque (for which the dimensionless function of  $\hat{\epsilon}$  converges when  $\hat{\epsilon} \rightarrow 0$ ) or for the differential Lindblad torque, it is a risky exercise in the case of the adiabatic torque excess, since the approximate expression of Eq. (95) diverges for  $\hat{\epsilon} \rightarrow 0$ . For the setup that we consider, we have tried to perform calculations at higher resolution and smaller smoothing lengths. The smallest smoothing length for which we have a steady situation is  $\epsilon = 0.07H$  (corresponding to the left square in Fig. 13). Under this value, we end up with very messy, unsteady situations, in which the flow is strongly affected by the presence of numerous vortices which drift along the separatrices. We can therefore only provide a conservative estimate of Eq. (97), by truncating the integral at  $\hat{\epsilon} = 0.07$ . We obtain:

$$\Gamma_1^{3D} \approx 2.8\mathcal{S}\Gamma_0.\tag{98}$$

In order to estimate the total torque in the three-dimensional case, we need to know the differential Lindblad torque, and the vortensity related part of the horseshoe drag. The first of those is given by Tanaka et al. (2002), and is, with our notation:

$$\Gamma_{LR} = -(2.34 - 0.1\alpha)\Gamma_0,\tag{99}$$

for a disk without a temperature gradient. We note that we do not use the total torque value given by Tanaka et al. (2002), but only the differential Lindblad torque. The total torque value contains indeed the linear corotation torque, which is not the corotation torque exerted in steady state (Paardekooper & Papaloizou 2009a). Instead, we consider separately the vortensity related horseshoe drag, and apply to it a treatment similar to

that of Eq. (97), which is straightforward in this case, because of the absence of divergence when  $\hat{\epsilon} \rightarrow 0$ . The two-dimensional component of the horseshoe drag that scales with the vortensity gradient reads (Ward 1991; Masset 2001):

$$\Gamma_V = \frac{3}{4} \mathcal{V} C^4(\hat{\epsilon}) \Gamma_0, \quad (100)$$

hence its three-dimensional estimate is:

$$\Gamma_V^{3D} \approx \frac{3}{\sqrt{8\pi}} \mathcal{V} \Gamma_0 \int_0^{+\infty} e^{-\hat{\epsilon}^2/2} C^4(\hat{\epsilon}) d\hat{\epsilon} \approx 0.93 \mathcal{V} \Gamma_0, \quad (101)$$

where we have used the series  $SI_i$  to tabulate  $C(\hat{\epsilon})$ . The total torque acting on a low-mass planet in a three-dimensional disk reads therefore:

$$\Gamma = [-(2.34 - 0.1\alpha) + 0.93\mathcal{V} + 2.8\mathcal{S}] \Gamma_0, \quad (102)$$

where we recall that the last term is a conservative estimate, and is likely to actually have a numerical coefficient larger than 2.8. We see that for  $|\mathcal{S}| \sim |\mathcal{V}| \sim 1$ , the term associated to the entropy gradient dominates the horseshoe drag, hence the adiabatic torque excess should efficiently halt or reverse migration in disks with moderate, negative entropy gradients, in agreement with the result of Paardekooper & Mellema (2006), who found that planetary migration can indeed be reversed in a three-dimensional disk.

## 8. Discussion

In this section we describe some side results, and we draw a list of points that deserve further investigation.

### 8.1. Topology of the flow and location of the stagnation point

As stated in section 2.4, we have assumed in this work that there is only one X-point in the vicinity of the planet. We find that this is indeed the case in most situations. We can

nevertheless get two X-points in the vicinity of the planet, if one of the following conditions is fulfilled:

- the entropy gradient vanishes, or is very small,
- the softening length of the potential is very small,
- the flow has not reached a steady state and is observed before a U-turn time scale.

While the first and last conditions are not relevant to the present work, which assumes a steady state and a sizable entropy gradient, the second case has some importance, as it gives indications of what can happen near the equatorial plane in a three-dimensional case. In the cases in which we have two X-points that subsist during the whole simulation, we get very time-dependent torque values. This can be interpreted as entropy trapped in the small libration island defined by the two X-points. The perturbation of density associated to the entropy distribution, that librates in this island, gives rise to large torque variation, as it corresponds to material very close to the planet. We note that this is quite in contrast with what we have claimed in section 5.3, where we have argued that it is the vortensity perturbation that yields the bulk torque. Whereas this is true for the downstream horseshoe stripes which lie at some distance of the planet, here the planet lies within the libration island, and the fact that the density response is spread radially or not definitely matters. We also note that the present discussion offers a number of similarities with the discussion in paper I about the flow topology as a function of the temperature gradient and of the softening length, except that here it is the entropy gradient that plays a role, rather than the temperature gradient.

When the flow is observed at an early stage, it may display two X-stagnation points, which are generally not on the same separatrix. We observe that once the flow has settled in a steady state, it is the outermost stagnation point (the one that is on the separatrix

that lies further from corotation) that subsists. It turns out that this point lies behind the planet for  $\mathcal{S} < 0$ , and is in front of the planet for  $\mathcal{S} > 0$ . While this fact is unimportant for a planet in fixed circular orbit, where only the distance of the stagnation point to the planet matters to evaluate the torque excess, it is crucial when the planet migrates, as the stagnation point is shifted from the position that it has on a fixed circular orbit. The consequences of this are discussed in the next section.

## 8.2. Feedback on migration

Since the adiabatic torque excess depends on the flow properties at the stagnation point of the horseshoe region, and since, as we shall see below, the location of the latter depends on the drift rate, we expect that a feed back loop can be established between the total torque and the migration rate, much as in type III migration (Masset & Papaloizou 2003). Contrary to type III migration, however, the feed back should generally be negative, therefore acting to decrease the absolute value of the drift rate. It should also be of relatively minor importance, except in very massive disks, with Toomre’s  $Q$  parameters close to unity. Consider the following numerical experiment: we repeat the runs SA<sub>10</sub> and SI<sub>10</sub>, except that we impose an inwards disk drift  $\dot{r}_d = -1.9 \cdot 10^{-5}$ . We note that, if the planet was allowed to freely migrate in run SA<sub>10</sub>, it would do so at the rate  $\dot{a} = 1.9 \cdot 10^{-5}$ . Rather than releasing the planet, we impose an inwards drift of the disk, of same magnitude. This technique has already been used for type III migration (see Masset & Papaloizou 2003, section 5.6). We see in Fig. 14 that the torque in the isothermal case does not depend on the drift rate, while there is a noticeable difference in the adiabatic case, and that the torque tends towards a somehow smaller value. The reason for this can be understood from the profile of radial velocity at corotation, depicted in Fig. 15. If the planet migrates outwards, the stagnation point (in a frame that moves radially with the planet) is located where the

horseshoe dynamics endows fluid elements with a radial velocity equal to that of the planet (similarly, if the planet is kept fixed, the new stagnation point is expected to lie where the radial velocity in the initial case is  $-\dot{r}_d$ .) Since fluid elements move outwards behind the stagnation point, the azimuth of the stagnation point decreases, hence the latter recedes from the planet, since it is located behind the planet in the case considered. A consequence of this recession is a lower perturbed pressure at the new position of the stagnation point, hence a lower value of the adiabatic torque excess. A similar decrease (in absolute value) is also expected in the case  $\mathcal{S} > 0$ . The stagnation point is then in the front of the planet (see section 8.1), and the total torque acting on the latter is negative. The stagnation point in the migrating case is therefore expected where the horseshoe U-turns are performed inwards, that is to say at the front of the stagnation point of the fixed case, and therefore further again from the planet. We have checked this with additional simulations, not reproduced here.

A number of comments are in order:

- Fig. 15 shows a poor agreement between the radial velocity for the disk’s drift case and the original radial velocity offset by  $-\dot{r}_d$ , in the region of the stagnation point ( $-0.07 \leq \phi \leq -0.03$ ). This is presumably due, at least in part, to the resolution of the grid. The direction of the shift of the stagnation point, and its order of magnitude, are nevertheless compatible with the new stagnation point being determined by the location where, in the initial flow,  $v_r = \dot{a}$ .
- Since both  $v_r$  and  $\dot{a}$  scale with the planet mass (for the range of planetary masses considered here), the shift of the stagnation point should not depend on the planetary mass.
- Since  $\dot{a}$  scales with the disk mass, the shift of the stagnation point of a freely migrating planet should increase with the disk mass. The magnitude of this effect, for the disk

considered in the numerical experiment described above, is at about  $1/20^{\text{th}}$  of the total torque. The disk has a Toomre parameter  $Q \approx 8$ . This shows that the effect we describe is of marginal importance, except in the most massive disks, for which  $Q \gtrsim 1$ .

- The drift rate in steady state is given by:

$$2Ba\dot{a} = \gamma + \frac{\partial\gamma}{\partial\dot{a}}\dot{a}, \quad (103)$$

where we assume that the torque excess, to lowest order, has an affine dependence on  $\dot{a}$ , and where  $\gamma$  is the specific torque acting on the planet. We therefore obtain:

$$\dot{a} = \frac{\gamma}{2Ba - \partial\gamma/\partial\dot{a}}. \quad (104)$$

In the particular case described above, we have  $\partial\gamma/\partial\dot{a} \approx -0.05 \cdot 2Ba$ , hence the steady state drift is almost equal to that dictated by the torque value measured in the disk drift case (i.e. further iterations with a drift rate of the disk given by the new torque value would hardly change the result).

### 8.3. Extension to arbitrary temperature profiles

The analysis presented in this work suffers from a restriction very similar to the restriction of the isothermal case, which is that the temperature profile is assumed to be flat. We have nevertheless performed many additional calculations in which we relaxed this constraint, and found that our main results essentially hold in disks with arbitrary temperature profiles:

- The global torque excess, defined by Eq. (57), scales with the entropy gradient. The isothermal runs which we use to apply Eq. (57) in the general case have same profiles as their adiabatic counterparts, hence they are locally isothermal runs, which

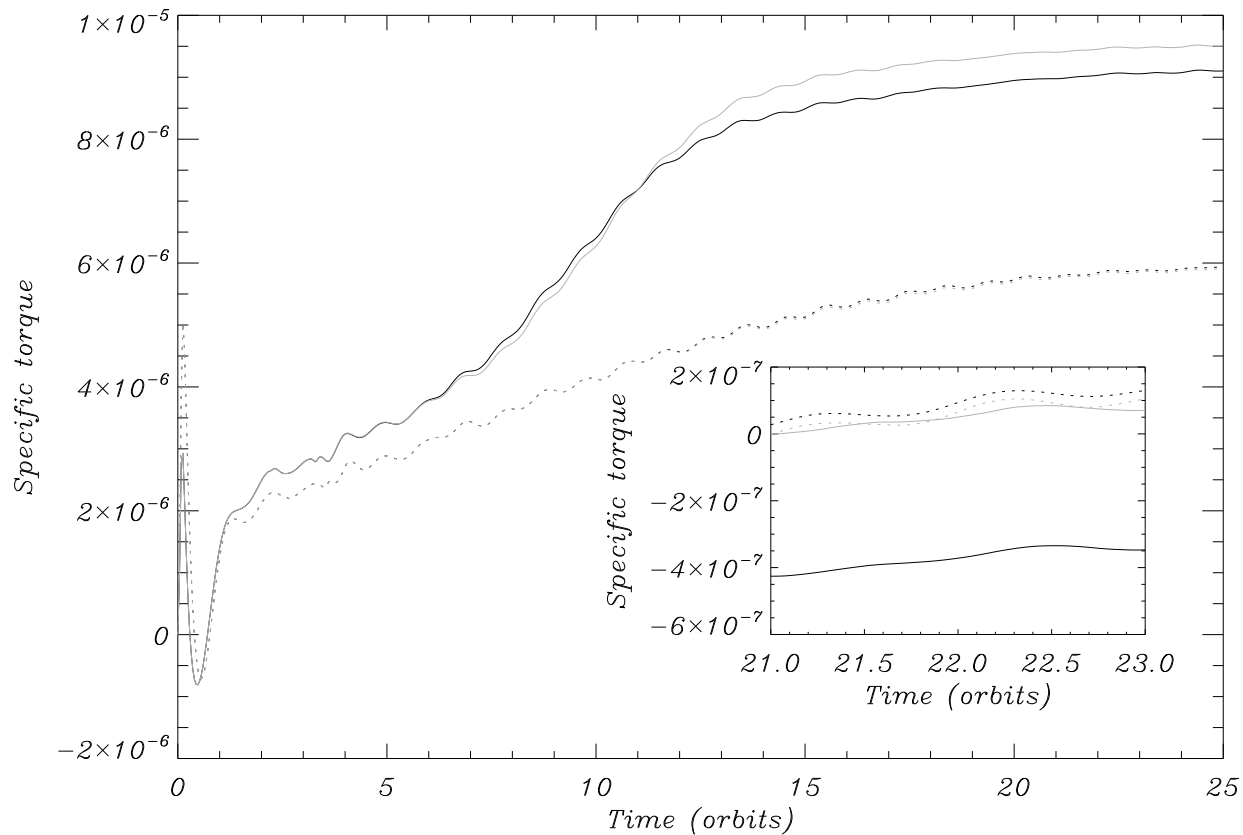


Fig. 14.— Specific torque on planet in the runs with an inwards disk drift. The solid line shows the adiabatic case and the dotted line shows the isothermal case. Grey curves show the initial runs (without disk drift). The inset plot shows a close up on the curves (the value of the torque at  $t = 21$  orbits in the case without disk drift has been subtracted to improve legibility).

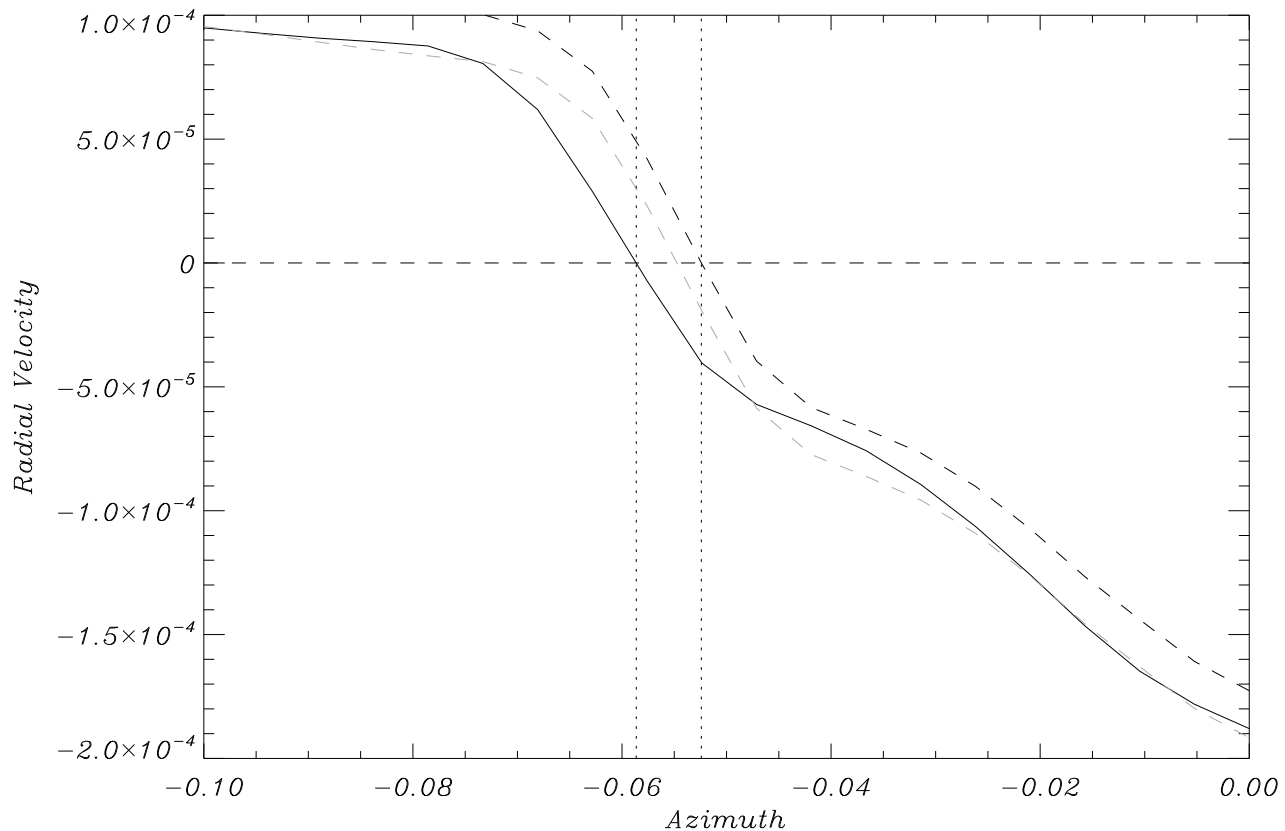


Fig. 15.— Radial velocity as a function of the azimuth, at  $r = r_c$ , in the static case (dashed line), and in the case with disk drift (solid line). The grey dashed curve shows the curve of the static case offset of  $\dot{r}_d$ . The rightmost vertical dotted line shows the initial location of the stagnation point, while the leftmost one shows the location of the stagnation point in the case with a disk drift, which is also the location expected for a planet moving outwards in the non drifting disk.

have singular evanescent waves excited at the separatrices, contrary to the globally isothermal runs (see paper I). These components, which scale with the temperature gradient, should therefore be also present in the general, adiabatic case.

- The half width of the horseshoe region exhibits the same characteristic V-shaped dependence on  $\mathcal{S}$ , as shown in Fig. 3.

The adiabatic torque excess, as a function of the entropy gradient, displays little scatter, and is therefore essentially a one-to-one correspondence. The results presented here can therefore be used to predict the torque in a general situation, provided the torque is known in the corresponding locally isothermal case.

#### 8.4. Adiabatic excess in turbulent disks

The analysis presented above relies upon the existence of a steady state and on that of a unique stagnation point. It therefore does not apply to the case of a turbulent disk. The adiabatic excess has been interpreted, however, as due to a constitutive asymmetry of the horseshoe region, acquired by the upstream flow under the action of the pressure gradient on overdense or underdense regions. To some extent, this effect should therefore persist in a turbulent disk, since we expect to find, in a turbulent disk, regions that are, in average, under- or over-dense with respect to the barotropic case, as a consequence of the advection of entropy. This issue deserves significant further work, since most of the regions of the disks where planetary migration is supposed to take place should be turbulent. In particular, it would be of interest to know whether the time-averaged torque excess is equal to the steady state estimate.

### 8.5. Saturation issues

In the absence of any process that can transfer angular momentum between the horseshoe region and the rest of the disk, the horseshoe drag is bound to saturate. A non-vanishing time averaged value of this torque would indeed imply a sustained transfer of angular momentum from the planet to the horseshoe region, where it would accumulate. Viscous torques, exerted at the separatrices between the horseshoe region and the outer or inner disk, can ensure this transfer of angular momentum (Masset 2001). In the case of an isothermal disk, viscous diffusion tends to restore the large scale gradient of vortensity across the horseshoe region. If it can do so in less than a libration time, the vortensity upstream of the horseshoe U-turn is that of the unperturbed disk, and the horseshoe drag is permanently equal to its initial value. In the case of an adiabatic flow, the vortensity related part of the horseshoe drag follows the same picture, and a sufficiently large viscosity is required to avoid the saturation of this component of the drag. The adiabatic torque excess, however, results from the advection of entropy, and to the existence, at the stagnation point, of a discontinuity of the entropy brought from the inside and from the outside. Sustaining the torque excess therefore implies that the discontinuity of entropy at the stagnation point is maintained. Paardekooper & Papaloizou (2008) consider thermal diffusion as the dissipative process that fulfills this function, while Kley & Crida (2008) consider realistic radiative effects. In both cases there can be a sustained, positive torque acting on the planet. We note however:

- that in any case a finite amount of viscosity is required. Thermal diffusion or radiative effects, which do not feature in Euler’s equation, cannot ensure the transfer of angular momentum out of the horseshoe region.
- That there is no theoretical expression of the steady state horseshoe drag that takes into account the balance between saturation and the dissipative processes that prevent

it. Such an expression is definitely required for planet population synthesis based on one-dimensional models of migration.

We also comment that, while saturation can be interpreted as the phase mixing of the contribution of different horseshoe streamlines in the barotropic case (Balmforth & Korycansky 2001), the case of the adiabatic torque excess is slightly different because there is essentially one streamline involved in this excess: the separatrix. It is therefore possible that the torque excess oscillates over a very long time, or indefinitely. Numerical simulations show that the oscillations of the torque damp after a few libration times (Baruteau 2008). It is not clear, however, whether this is a physical effect or the consequence of numerical diffusivity. This again appeals for the need of simulations at very high resolution.

We finally mention the systematic appearance of a vortex at one of the downstream separatrices (the one that has a negative singularity of vorticity). It would be of interest to study the impact of this vortex on the saturation of the adiabatic excess. On the one hand, it provides a mixing of the entropy in the vicinity of the separatrix, and on the other hand, it may assist the horseshoe region in exchanging angular momentum with the rest of the disk.

## 9. Conclusions

We have shown that the horseshoe drag exerted on a low-mass planet, embedded in a disk that behaves adiabatically on the time scale of a horseshoe U-turn, can be considered as the sum of two terms:

- a bulk term, involving all the horseshoe streamlines, which necessarily scales with the vortensity gradient, exactly as in a barotropic disk. This is in agreement with the forecast made in the introduction: there is no room, for a generic horseshoe

streamline, for an exchange of angular momentum with the planet different from that of a barotropic situation.

- An edge term, which manifests itself as a torque excess with respect to the barotropic case. This term scales with the radial gradient of entropy, and it corresponds to a constitutive asymmetry of the horseshoe region. In a pressureless disk, this asymmetry would trigger the appearance of underdense or overdense thin stripes of gas at the downstream separatrices. In a gaseous disk, pressure forces spread radially these stripes by the excitation of evanescent waves, leaving imprints as vorticity sheets at the separatrices as the most tangible manifestation of this effect.

The origin of the adiabatic torque excess is therefore not the conspicuous under- or over-dense regions that appear within the horseshoe region and which are bound by a contact discontinuity at the downstream separatrices, as originally thought. Instead it is due to rather discreet single evanescent waves launched at the downstream separatrices. This answers some issues arising from earlier works. In particular, no adiabatic torque excess is expected in the limit of a cold disk (Baruteau & Masset 2008), whereas the contact discontinuities still exist in this limit and delineate perturbations of finite mass. The torque excess that we find scales with the perturbed pressure at the horseshoe’s stagnation point, hence it vanishes in the limit of a cold disk.

We found a number of side results:

- The horseshoe region in the adiabatic case has a more complex dependence on the disk’s parameters than in the barotropic case. In particular, the horseshoe region is wider than expected from barotropic estimates, when there is a non-vanishing entropy gradient. A consequence of this effect is that the bulk horseshoe term, that scales with the vortensity gradient, is boosted with respect to its value in a barotropic disk. This

effect is relatively weak, however, and most of the difference between the adiabatic and barotropic case comes from the edge term, in disks with realistic profiles.

- The adiabatic torque excess slightly depends on the migration rate. There is therefore a weak feed back on migration. This feed back is found to be generally negative (i.e. it tends to lower the drift rate, either inward or outward), and is virtually negligible except in very massive disks.

We find that even at relatively high resolution, numerical simulations may mistakenly locate the stagnation point, which has some impact on the torque excess value. We therefore stress the need for very high resolution calculations, for which nested mesh codes would be a valuable tool. In a similar vein, the steep dependence of the excess on the potential's softening length suggests that the effect can be very strong in the three dimensional case. This issue requires significant further work.

The numerical simulations performed in this work have been run on the 92 core cluster funded by the program *Origine des Planètes et de la Vie* of the French *Institut National des Sciences de l'Univers*. Partial support from the COAST project (*COmputational ASTrophysics*) of the CEA is also acknowledged. The authors also wish to thank G. Koenigsberger for hospitality at the Instituto de Ciencias Físicas of UNAM, Mexico, and acknowledge partial support from CONACYT project number 24936. The authors are grateful to S. Fromang and C. Baruteau for a thorough reading of a first draft of this manuscript.

### A. Expression of the pressure perturbation

The convolution product of the rectangular function

$$R : x \mapsto \begin{cases} 1 & \text{if } 0 < x < x_0 \\ 0 & \text{otherwise,} \end{cases} \quad (\text{A1})$$

by the kernel  $K(x) = \exp(-|x|/\lambda)/(2\lambda)$  is:

$$\tilde{R}(x, x_0, \lambda) = \begin{cases} 1 - \exp\left(-\frac{x_0}{2\lambda}\right) \cosh\left(\frac{x - x_0/2}{\lambda}\right) & \text{if } x \in [0, x_0], \\ \exp\left(-\frac{x - x_0/2}{\lambda}\right) \sinh\left(\frac{x_0}{2\lambda}\right) & \text{otherwise.} \end{cases} \quad (\text{A2})$$

Similarly, the convolution product of the triangular function

$$T : x \mapsto \begin{cases} x & \text{if } 0 < x < x_0 \\ 0 & \text{otherwise,} \end{cases} \quad (\text{A3})$$

by the kernel  $K(x) = \exp(-|x|/\lambda)/(2\lambda)$  is:

$$\tilde{T}(x, x_0, \lambda) = \begin{cases} \frac{\exp(x/\lambda)}{2} \left[ -(x_0 + \lambda) \exp\left(-\frac{x_0}{\lambda}\right) + \lambda \right] & \text{if } x < 0, \\ \frac{\exp(-x/\lambda)}{2} \left[ (x_0 - \lambda) \exp\left(\frac{x_0}{\lambda}\right) + \lambda \right] & \text{if } x > x_0, \\ x + \frac{\lambda}{2} \exp\left(-\frac{x}{\lambda}\right) - \frac{x_0 + \lambda}{2} \exp\left(\frac{x - x_0}{\lambda}\right) & \text{if } x \in [0, x_0]. \end{cases} \quad (\text{A4})$$

Using Eq. (81), we obtain:

$$\delta P = -\frac{\Gamma_1 c_s^2}{(8a|A|Bx_s^2) \cdot (2\gamma^{1/2}H)} \exp\left(-\frac{|x|}{\sqrt{\gamma}H}\right) - \frac{2\Sigma_0 c_s^2}{r_p} (\mathcal{S} + \mathcal{V}) \tilde{T}(x, x_s, \sqrt{\gamma}H) \quad (\text{A5}) \\ + \Sigma_0 c_s^2 \frac{\delta l_{\text{prod}}}{l_0} \tilde{R}(x, x_s, \sqrt{\gamma}H),$$

where we have also made use of Eq. (62) to transform the first term.

## REFERENCES

- Balmforth, N. J., & Korycansky, D. G. 2001, *MNRAS*, 326, 833
- Baruteau, C. 2008, PhD thesis, Ecole Doctorale d’Astronomie et d’Astrophysique d’Ile de France, Observatoire de Paris, F-75014, Paris, France
- Baruteau, C., & Masset, F. 2008, *ApJ*, 672, 1054
- de Val-Borro, M., Edgar, R. G., Artymowicz, P., Ciecielag, P., Cresswell, P., D’Angelo, G., Delgado-Donate, E. J., Dirksen, G., Fromang, S., Gawryszczak, A., Klahr, H., Kley, W., Lyra, W., Masset, F., Mellema, G., Nelson, R. P., Paardekooper, S.-J., Peplinski, A., Pierens, A., Plewa, T., Rice, K., Schäfer, C., & Speith, R. 2006, *MNRAS*, 695
- Kley, W. 1998, *A&A*, 338, L37
- Kley, W., & Crida, A. 2008, *A&A*, 487, L9
- Lovelace, R. V. E., Li, H., Colgate, S. A., & Nelson, A. F. 1999, *ApJ*, 513, 805
- Masset, F. 2000a, *A&AS*, 141, 165
- Masset, F. S. 2000b, in *Astronomical Society of the Pacific Conference Series*, Vol. 219, *Disks, Planetesimals, and Planets*, ed. G. Garzón, C. Eiroa, D. de Winter, & T. J. Mahoney, 75–+
- Masset, F. S. 2001, *ApJ*, 558, 453
- . 2002, *A&A*, 387, 605
- Masset, F. S., D’Angelo, G., & Kley, W. 2006, *ApJ*, 652, 730
- Masset, F. S., & Papaloizou, J. C. B. 2003, *ApJ*, 588, 494
- Morohoshi, K., & Tanaka, H. 2003, *MNRAS*, 346, 915

- Paardekooper, S.-J., & Mellema, G. 2006, *A&A*, 459, L17
- Paardekooper, S.-J., & Papaloizou, J. C. B. 2008, *A&A*, 485, 877
- . 2009a, *MNRAS*, 394, 2283
- . 2009b, *MNRAS*, 394, 2297
- Tanaka, H., Takeuchi, T., & Ward, W. R. 2002, *ApJ*, 565, 1257
- Ward, W. R. 1986, *Icarus*, 67, 164
- Ward, W. R. 1991, in *Lunar and Planetary Institute Conference Abstracts*, 1463–+
- Ward, W. R. 1992, in *Lunar and Planetary Institute Conference Abstracts*, 1491–+
- . 1997, *Icarus*, 126, 261